



ELSEVIER

Contents lists available at SciVerse ScienceDirect

# Ocean Engineering

journal homepage: [www.elsevier.com/locate/oceaneng](http://www.elsevier.com/locate/oceaneng)

## A wave parameters and directional spectrum analysis for extreme winds

R.D. Montoya<sup>a,b,\*</sup>, A. Osorio Arias<sup>b</sup>, J.C. Ortiz Royero<sup>c</sup>, F.J. Ocampo-Torres<sup>d</sup><sup>a</sup> Programa de Ingeniería Civil, Universidad de Medellín, Carrera 87 N° 30-65, Medellín, Colombia<sup>b</sup> Grupo de Oceanografía e Ingeniería Costera (OCEANICOS), Universidad Nacional de Colombia Sede Medellín, Carrera 80N° 65-223, Medellín, Colombia<sup>c</sup> Grupo de Física Aplicada, Dpto. de Física. Instituto de Estudios Hidráulicos y Ambientales IDEHA, Universidad del Norte, km 5 Vía Puerto Colombia, Barranquilla, Colombia<sup>d</sup> Centro de Investigación Científica y de Educación Superior de Ensenada, Carretera Tijuana-Ensenada, 3918 Ensenada, BC 22860, México

### ARTICLE INFO

#### Article history:

Received 28 April 2012

Accepted 6 April 2013

Available online 16 May 2013

#### Keywords:

Wind speed  
Directional spectrum  
Gulf of Mexico  
Moored buoys  
Hurricane waves

### ABSTRACT

In this research a comparison between two of the most popular ocean wave models, WAVEWATCH III<sup>TM</sup> and SWAN, was performed using data from hurricane Katrina in the Gulf of Mexico. The numerical simulation of sea surface directional wave spectrum and other wave parameters for several parameterizations and its relation with the drag coefficient was carried out. The simulated data were compared with in-situ NOAA buoy data. For most of the buoys, WAVEWATCH III<sup>TM</sup> presented the best statistical comparisons for the main wave parameters, such as significant wave height and peak period. The SWAN model tends to overestimate the maximum values for significant wave height for some buoys and the peak period for almost all the buoys. Both models tend to overestimate the value of peak direction, presenting an area of greater energy to the south. The WAVEWATCH III<sup>TM</sup> model performs best for buoys located in right forward quadrant, which generally has higher winds and waves. This indicates a better spatial representation of wave parameters in the higher energy areas for the WAVEWATCH III<sup>TM</sup> model. Results based on the quadrant location for most of the analyzed cases, are in agreement with the results from other sources such as the Scanning Radar Altimeter (SRA).

© 2013 Elsevier Ltd. All rights reserved.

### 1. Introduction

Knowledge of directional wave characteristics is important for several topics of research, such as: physical interactions between wind and ocean waves that are reflected in the shape of the directional wave spectrum, understanding of the complex wind and swell systems and their relationship with the design and operational safety of marine structures (harbors, ships, and offshore structures), coastal processes, wave-induced erosion among others.

During hurricane conditions, intense and fast-varying wind forcing produces severe and complex ocean wave fields varying in space and time, which can propagate for thousands of kilometers from the storm center (Barber and Ursell, 1948; Moon et al., 2003; Zhuo et al., 2008). The directional wave spectrum describes the complex and chaotic phenomenon of wind-generated ocean waves in terms of contributions from waves propagating in different directions with different wavelengths (Khama et al., 2003).

As reported by several authors, spatial and temporal variations of directional spectrum during hurricane conditions are strongly dependent on the relative position from the hurricane eye and the hurricane translation speed. The hurricane wind field is typically asymmetric due to the hurricane movement. Winds and waves are generally stronger to the right (and so weaker to the left) of the hurricane because the forward velocity of the storm adds to the wind velocity around the eye (Moon et al., 2003; Zhuo et al., 2008; Wright et al., 2001; Xu et al., 2007).

Some authors have validated the behavior of models such as Simulating Waves Nearshore (SWAN) and WAVEWATCH III<sup>TM</sup> (WWIII) to reproduce the directional wave spectrum during hurricane conditions and the main characteristics of directional spectrum from other sources. Although the SWAN model was developed for coastal areas, as seen in version (40.11), spherical coordinates have been included in the code for oceanic applications (Ortiz and Mercado, 2008).

Moon et al. (2003) performed a numerical simulation of sea surface directional wave spectrum for Hurricane Bonnie (1998) using the WWIII model with a high-resolution. The results were compared with buoy observations and NASA Scanning Radar Altimeter (SRA) data for directional spectrum. The results show that excluding shallow areas near the shore, the model yields an excellent simulation of the directional spectrum. It was concluded that the

\* Correspondence to: Medellín University, Civil engineering Program, Carrera 87 N° 30-65 (Bloque 4), Medellín, Suramérica, Colombia. Tel.: +57 4 3405555; fax: +57 4 3405555.

E-mail addresses: [rmontoya@udem.edu.co](mailto:rmontoya@udem.edu.co), [rdmontoya1@gmail.com](mailto:rdmontoya1@gmail.com) (R.D. Montoya).

hurricane-generated wave field is mostly determined by two factors: the distance from the hurricane center and hurricane translation speed. Zhuo et al. (2008) compared directional spectrum from WWIII during Typhoon Damrey (2005) with directional spectrum from buoy observations in the Northwest Sea area of Hainan Island. Their results agree with those presented by Moon et al. (2003).

Young (2006) studied the directional wave spectrum produced by the passing of several hurricanes using wave buoy observations and showed that in almost all quadrants of the storm, the dominant waves are remotely generated swells. Such results indicate that the spectral shape is controlled almost completely by non-linear interactions with input and dissipation terms of less importance. This illustrates that input and dissipation are important in determining the total quantity of energy in the wave field, but appear to play only a minor role in determining the spectral shape.

Given the importance of detailed directional wave data and the lack of information available capable of representing their spatial and temporal variability, ocean wave modeling is a very useful and convenient way to obtain the spatial and temporal distribution of directional spectrum (Zhuo et al., 2008). Actually, there are few studies that compare the characteristics of directional spectrum produced by different models during hurricane conditions, against the most popular and available directional spectrum data from NDBC buoys and its relation with quadrant location. The results obtained are of vital importance for engineering applications in which the directional wave spectrum plays an important role.

The blended wind methodology proposed by Montoya et al. [Comparison of several reanalysis data sets combined with the hurricane wind model HURWIN: Methodology to improve wind field during hurricane conditions. Manuscript in preparation] to reconstruct the wind field during hurricane conditions, observations from NOAA buoys and Surface Wind Analysis from the Hurricane Research Division (HRD) were used in this study. These methods and data were employed to investigate the directional spectrum performance of two of the most popular wind wave models, WWIII (Tolman and Chalikov, 1996 and Tolman, 2002, 2009) and SWAN (Ris et al., 1994, 1999; Booij et al., 1996; Booij et al., 1999; Holthuijsen and Booij, 2003; Booij, 2004) during

hurricane conditions. The quality of the main statistical wave parameters when compared with in-situ data and a brief discussion about the possible shortcomings related to the method employed by the NDBC to obtain the directional spectrum were also looked at based on the literature review.

The datasets used in the present study include NOAA-NDBC buoys 42001, 42002, 42003, 42007, 42019, 42035, 42038, 42039 and 42040 located in the Gulf of Mexico, wind data from the North American Regional Reanalysis – NARR data set (Mesinger et al., 2006), aircraft hurricane best tracking information from National Hurricane Center available at <http://www.nhc.noaa.gov>.

This paper is organized as follows. Section 2 presents a description of the data sets employed and the study area. A brief outline about the WWIII, SWAN and HURWIN models and blended wind methodology is given in section 3. Using NOAA in-situ buoys, Section 4 compares the main wave parameters for both models and a comprehensive comparison of the directional and frequency wave spectrum is presented. Results are based on the distance from the hurricane eye and the quadrant location. The summary and conclusions are given in the last section.

## 2. Study area and data set description

The Gulf of Mexico is located at the southeastern corner of North America approximately between 18°N and 31°N and 80°W to 98°W. It has a surface area of about 1,500,000 square kilometers and is bounded in the north by the United States, in the southwest and south by Mexico, and in the southeast by Cuba. Approximately 38% of the gulf is comprised of shallow and intertidal areas (< 20 m deep). The continental shelf (< 180 m deep) represents approximately 22% of the area and the other 40% is comprised of a variety of deeper waters. The bathymetry was obtained from the 2-min Gridded Global Elevation Data set (ETOPO-2) available at: [http://www.ngdc.noaa.gov/mgg/gdas/gd\\_designagrid.html#](http://www.ngdc.noaa.gov/mgg/gdas/gd_designagrid.html#) (see Fig. 1).

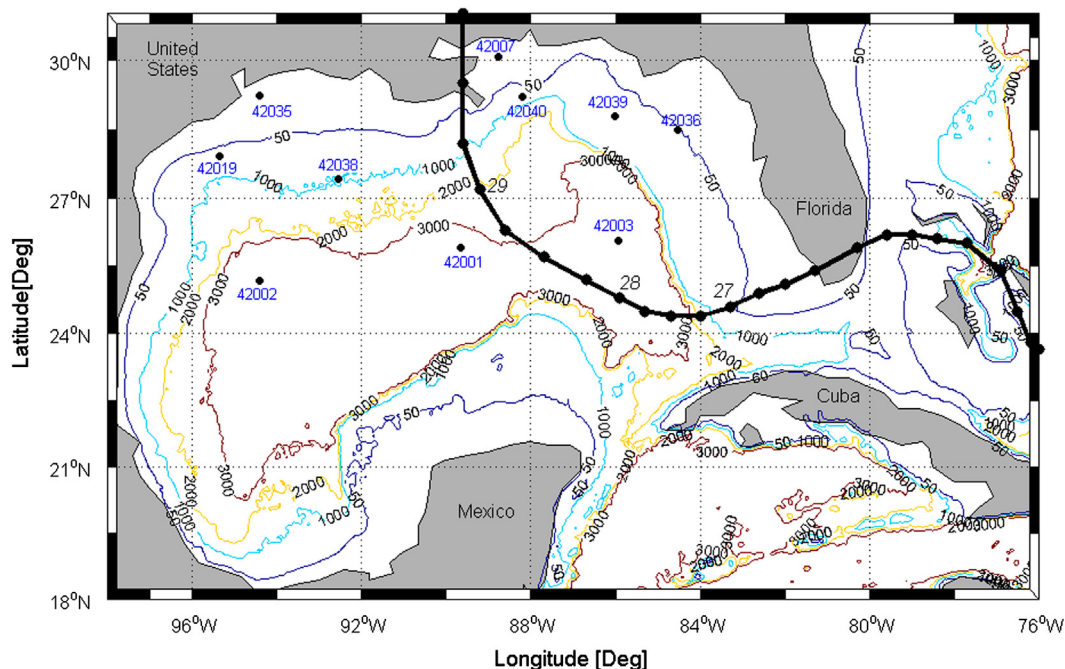


Fig. 1. Katrina's track and buoy locations in the Gulf of Mexico.

**Table 1**  
Characteristics of buoys located in the Gulf of Mexico.

Buoy	Coord		years	Anemo height [m]	Buoy Type	Water depth [m]
	Long East	Lat North				
42001	-89.67	25.90	Since 1975-P	10	Dir	3246.0
42002	-94.41	25.17	Since 1973-P	10	Dir	3566.0
42003	-85.94	26.07	Since 1976-P	5	Dir	3282.0
42007	-88.77	30.09	Since 1981-P	5	Dir	13.7
42019	-95.36	27.91	Since 1990-P	5	Dir	83.9
42035	-94.41	29.23	Since 1990-P	5	Dir	13.7
42036	-84.52	28.50	Since 1994-P	5	Dir	54.5
42038	-92.56	27.42	Since 2004-P	5	Dir	1152.0
42039	-86.01	28.79	Since 1995-P	5	Dir	307.0
42040	-88.21	29.21	Since 1995-P	5	Dir	274.0

Notations: P=Present, Dir=Directional Buoy.

### 2.1. Buoy data and directional spectrum description

The observed in-situ wind and wave data were obtained from the NOAA National Data Buoy Center (NDBC) from operational buoys, available at: <http://www.ndbc.noaa.gov/>. Table 1 shows the main buoy characteristics.

The buoys employed were selected considering the available data and spatial distribution. The main variables used correspond to h level eight-minute average wind speed (WSPD) values in m/s, reported hourly. For buoys with an anemometer height (h) equal to five meters, high wind speed values were corrected employing an iterative method that used a logarithm profile and the results obtained by Powell et al. (2003). It considered the variability of the following relevant surface layer quantities: sea surface roughness length (Z0), friction velocity ( $U^*$ ), neutral stability 10-m wind speed (U10) and the drag coefficient (Cd). Results from Powell et al. (2003) and a number of studies suggest that for high wind speeds (greater than 35–40 m/s) the drag coefficient decreases (Moon et al. 2003; Moon et al., 2004a; Moon et al., 2004b; Moon et al., 2004c; Makin, 2005; Kudryavtsev and Makin 2011; among others). WDIR wind direction refers to where the wind is coming from true north, in degrees clockwise, during the same period used for WSPD (WD). WVHT significant wave height (Hs) in meters was calculated as the average of the highest one-third of all wave heights recorded during the 20-minute sampling. DPD (Peak period, Tp) dominant wave period in seconds was calculated as the period with the maximum wave energy. MWD refers to the direction from which the waves at the dominant period (DPD) are coming (Dirp), in degrees from true north. Directional spectrum was obtained with the following expression  $S(f,\theta)=C11*D(f,\theta)$ , where C11=spectral wave density or nondirectional spectrum, f=frequency [Hz],  $\theta$ =Azimuth angle measured clockwise from north to the direction the wave is coming from [Deg]. D(f, $\theta$ ) is a directional spreading function available at <http://www.ndbc.noaa.gov/> obtained using the R1,R2,( $\alpha$ 1) ALPHA1 and ( $\alpha$ 2) ALPHA2 as the first and second normalized polar coordinates of the Fourier coefficients and the mean and principal wave directions.

The main purpose of this research was not to discuss which of the existing methods for estimating the directional spectrum is the most appropriate. However, a brief summary of the most important aspects found by different authors regarding the quality of the directional spectrum based on the method employed is presented. Some important aspects of the various instruments, measurement techniques, methodologies and other features should be considered for a proper understanding of the differences between the directional spectrum obtained by the NDBC buoys and numerical models. This may be very important for engineering applications when considering that assumptions based on only two

parameters such as wave height and wave period can lead to significant errors.

First, the directional spectrum can be obtained from records in a specific area of the sea recorded by a wide variety of sensors, arrays and platforms. Instrumental design and selection are fundamentally dependent on weather characteristics of the area, which define the wave climate conditions. Areas where the predominant wind direction is known need different instrumentation from those areas with high wind direction variability. For NDBC buoys, different systems and data acquisition methods are available (approximately seven (7) types of payloads and 6 types of platforms). For the buoys used in this study located in the Gulf of Mexico, six (6) are 3 m discus buoys (42001, 42003, 42007, 42019, 42035, 42039) and only two (2) are 10 m discus buoys (42002, 42040). Regarding the NDBC payloads, three (3) buoys have the recent payload AMPS system (42001, 42003 and 42019) and five have the ARES system (42002, 42007, 42035, 42039 and 42040).

The NDBC buoys measured nondirectional wave time series data consisting of digitized data from a single-axis accelerometer with its measurement axis perpendicular to the deck of the buoy in which it is mounted. For measured directional wave buoy pitch and roll information, data time series consisting of digitized data are required. These series represent one of the following types of data sets: (1) Buoys with nearly vertical acceleration, pitch (P(t), N–S slope), and roll (R(t), W–E slope), measured using a Datawell Hippy 40 sensor and incorporating a nearly vertical stabilized platform. A buoy azimuth obtained from measurements of the Earth's magnetic field recorded with a hull-fixed magnetometer. (2) Buoy acceleration measured from a single-axis accelerometer with its measurement axis perpendicular to the deck of the buoy in which it is mounted. Buoy pitch (P(t), N–S slope), roll (R(t), W–E slope), and azimuth obtained from measurements of the Earth's magnetic field with a hull-fixed magnetometer. (3) Buoy pitch (P(t), N–S slope) and roll (R(t), W–E slope), measured employing an Angular Rate System (ARS) (Earle, 1996). The Datawell Hippy sensor is expensive, heavy and large but has an excellent accuracy for measuring ocean waves (Steele et al., 1999). In contrast the (ARS) has a low price and good and improved accuracy. The (ARS) is the newest compact, low power Digital Directional Wave Module (DDWM) measurement system. This sensor uses the same wave data processing techniques, algorithms and software as those from earlier NDBC wave systems, but permit reduce operating costs (Chung-chu et al., 2009). Steele et al. (1999) shows the advantage to use less expensive tilt sensors for measure the pitch and roll data with fairly good results.

Possible problems related to the design of the buoys may appear because a discus hull cannot perfectly track the motion of waves with lengths comparable to, or less than, its diameter. Even when the waves are long enough, the inertia of the hull can prevent it keeping up with the heave and/or slope motions of the water surface. Furthermore, depending on the hull/mooring design, tension in the mooring line can prevent the hull from responding fully to the tilt of the wave (Steele and Wang, 2004). For rectify this problem, the NDBC routinely assume that the east and north deck slopes of a pitch-roll buoy respond to east and North Sea slopes as simple harmonic oscillators. However, Steele and Wang (2004) showed that substructures altering the main moments of inertia of the buoy along its principal axes can be a factor that slightly affects the validity of this assumption.

Another important factor that affects the directional wave spectrum accuracy is related to the method employed to calculate the directional wave energy spreading function D(f, $\theta$ ). For the NDBC buoys directional spectrum is estimated using a directional Fourier approach originally developed by Longuet-Higgins et al. (1963). For this method the cross-spectral parameters (C11, C22, C33, C23, Q12, Q13) are transformed into directional expansion parameters C11, r1,

$\alpha_1$  (ALPHA1),  $r_2$ ,  $\alpha_2$  (ALPHA2) as described above. C11 is the wave elevation spectral density (frequency spectrum), C22 is the E–W wave slope spectral density, C33 is the N–S wave slope spectral density, C23 is the co-spectral density, E–W and N–S are wave slopes, Q12 is the quadrature spectral density, elevation and E–W slope, Q13 is quadrature spectral density, elevation and N–S slope.

Although a directional Fourier series obtained with the Longuet-Higgins et al. (1963) expression, has poor directional resolution compared with advanced methods such as those based on the Maximum Likelihood Method (hereafter MLM) and Maximum Entropy Method (hereafter MEM), the MEM causes problems in that it produces artificial double peaks. In addition, the MEM has a narrower resolution than the MLM, as also found by other authors (Earle et al., 1999). For the utilized  $D(f,\theta)$  parameters, the half-power width of the weighting function is  $88^\circ$ . Longuet-Higgins et al. (1963) provide a weighting of the directional Fourier coefficients to prevent unrealistic negative values of  $D(f,\theta)$  for directions far from  $\theta_1$ , but this approach is not used by the NDBC because it increases the half-power width to  $130^\circ$  (Earle, 1996).

The methodology proposed by Longuet-Higgins et al. (1963) heavily filters the original, with a strongly increased directional spreading. However, the higher resolution methods such as MEM and MLM may provide erroneous directional information unless they are carefully applied (Earle, 1996), thus, they are not presently used by NDBC. Isobe et al. (1984) found that the MLM slightly underpredicts wave energy around the mean wave direction while it overpredicts energy around the opposite direction. This observation was also confirmed by Zhang and Zhang (2005), employing numerical tests. Using the MLM method, they proposed a new approach to estimate the directional spreading function and then the angular Fourier Coefficients for the Cosine-2s directional spreading model. They showed that the conventional method based on the Longuet-Higgins et al. (1963) theory is sensitive to errors when estimating the cross-spectra while the MLM is more tolerant to such errors.

Reilly et al. (1996), compared a Datawell Directional Waverider and widely used National Data Buoy Center 3-m discus buoy, against six pressure transducers mounted 14 m below the sea surface on a platform with 200 m of depth, and shows that the Hippy sensor is sensitive to trim errors and has low signal to noise ratios when measuring small sea surface slopes. However, translation systems such as the Datawell systems were seen to be more sensitive to restrictions of their horizontal movement. The results show that the directional spread obtained with the Datawell system was in good agreement with the platform array, while the NDBC buoy overpredicted directional spread by about 6 degrees. Numerical simulations show that pitch-roll buoys with levels of noise of 5% in either surface elevation or surface slope measurement, will not seriously affect estimates of mean direction, but will cause a positive bias in the directional spread.

For a 3 m (NDBC) discus buoy (44014) Wang and Freise (1997) showed that derived parameters were found to be quite small, calculated at less than 3% for the sea height and usually less than  $4^\circ$  for the peak wave direction. However, errors in the directional wave spectrum were found to be potentially significant. These errors are associated with the buoys only measuring sufficient

data for the first two terms of the Fourier expansion of the directional spectrum. Despite this, they show that approximately 60% of the sample of wave records gives an upper bound Root Mean Square Error (RMSE) of less than 30% of the RMSE energy of the spectrum, which may be sufficiently accurate for many research requirements.

The selection of a suitable method for data analysis depends on the instruments employed for measurements and heavily on the sea conditions at the site. A simple estimation method may be adequate for moderate spreading of wave energy due to normal wind speed and without the presence of swell, while a sophisticated estimation method is necessary when swell is present or when estimating at a site where frequent changes in wind direction may occur (Ochi, 1998).

## 2.2. Hurricane data

Hurricane Katrina was one of the most destructive and deadly hurricanes that had impacted the United States in decades. It occurred during the 2005 hurricane season in the Atlantic, and was the third strongest storm of the season. It first appeared as a tropical storm and reached category five in five days. The forcing of the hurricane wind model HURWIN described below was obtained from the best track information from National Hurricane Center available at <http://www.nhc.noaa.gov>. The information includes the position in latitude and longitude, maximum 1-minute surface wind speeds in knots, and minimum central pressure in millibars. Fig. 1 shows the location of all buoys in the Gulf of Mexico used in this study and the track of the hurricane Katrina. In Table 2 the main characteristics of the two buoys nearest to Katrina's track are shown.

## 2.3. North American Regional Reanalysis (NARR)

For the blended winds methodology, the North American Regional Reanalysis data set (NARR) was employed. NARR is in essence a high-resolution extension and enhancement of low-resolution global reanalysis I data set (NCEP/NCAR reanalysis I) developed by the National Center for Environmental Prediction NCEP and the National Center for Atmospheric Research NCAR. NARR employs a Regional Climate Data Assimilation System (R-CDAS) that is significantly better than the global NCEP/NCAR reanalysis (GR2) at capturing the regional hydrological cycle, the diurnal cycle and other important features of weather and climate variability (Mesinger et al., 2006). The assimilation system has a spatial resolution of 32 km approximately with a 3-hourly output in 29 vertical layers. The information is available at: <http://www.cdc.noaa.gov/data/gridded/data.narr.monolevel.html> in NetCDF format. The zonal and meridional wind U10, V10 information with 8-times daily available from 1979/01/01 to present was employed. The grid resolution is 349 rows  $\times$  277 columns, which is approximately  $0.33^\circ$  (32 km) resolution at the lowest latitude.

**Table 2**

Main characteristics of nearest buoys to the Katrina's track.

Hurricane	Category <sup>a</sup>	Nearest Buoy <sup>b</sup>	$R_{\max}$ <sup>c</sup> Hurricane [km]	Minimum Distance [km]	Date [mm/dd/yy]
Katrina	C5	42007	19.66	101.9	08/29/12UTC-2005
	C4	42003	17.45	115.5	08/28/06UTC-2005

<sup>a</sup> Based on Saffir Simpson classification.

<sup>b</sup> Less than 150 km.

<sup>c</sup> Based on Willoughby (2004).

### 3. Description of models

#### 3.1. Brief outline of wind wave models development

Based on the spectral decomposition concept and the wave energy balance equation expressed as a function of the directional spectrum, wind wave models have evolved throughout history as a result of scientific advances. The first generation models, which evolved in the 1960s and 1970s, are the simplest. They assume the growth of each wave spectral component (frequency and direction) independently and do not have an explicit nonlinear wave interaction term. This term is implicitly expressed through the wind input (obtained by Phillips, 1957, and Miles, 1957, who looked at the generation mechanism) and dissipation terms, which assumed that the wave components suddenly stopped growing as soon as they reached a universal saturation level (Phillips, 1958; ECMWF, 2009). The saturation spectrum, represented by the one-dimensional ( $\widehat{f}$ -5) frequency spectrum of Phillips and an empirical equilibrium directional distribution, was then created. It is widely recognized that the main shortcomings of these models are related to overestimating the wind input, being incompatible with the known total momentum transfer across the air–sea interface (Snyder and Cox, 1966), and disregarding or making a strong underestimation of nonlinear transfer (Massel, 1996; Komen et al., 1994).

Due to the problems presented by the first generation models regarding the adjustment of the energy equation, several studies related to the influence of wind input and nonlinear interactions on wave growth were developed (Mitsuyasu, 1968a, 1969; Hasselmann et al., 1973). These resulted in the appearance of second generation models by the early 1980s. In these new models the nonlinear interactions are parameterized in simple form. Shortcomings arise from the fact that the wind sea part of the spectrum must be predefined, and requires assumptions as to how the wind sea becomes swell and vice versa (both work almost independently). Second generation models included the “coupled hybrid” and “coupled discrete” formulations. These models therefore suffered basic problems regarding the nonlinear interactions (energy transfer) between wind sea and swell. For rapidly varying wind fields where a complex directional spectrum is generated, second generation models do not work properly.

The evolution of more sophisticated computers and methods for the estimation of nonlinear interactions (Hasselmann et al., 1985; Webb, 1978; Tracy and Resio, 1982 and Resio and Perrie, 1991) promoted the development of third generation models. In these models the wave spectrum was computed by the integration of the energy balance equation, without any prior restriction on the spectral shape. Third generation models explicitly represent all of the physics relevant for the development of the sea state in two dimensions (exact solution of the nonlinear interactions are included), improving energy transfer between the wind sea and swell. These can be usefully employed when the wind field is changing rapidly (e.g. during hurricane conditions).

Among these models is the WAM (Cycles 1–4) (WAMDI Group, 1988), WAVEWATCH III (Tolman and Chalikov, 1996 and Tolman, 2002, 2009) MRI-III (Ueno and Ishizaka, 1997) JWA3G (Suzuki and Isozaki, 1994) and SWAN (Ris et al., 1994; Ris et al., 1999; Booij et al., 1996; Booij et al., 1999; Holthuijsen and Booij, 2003; Booij, 2004),

#### 3.2. Third generation wave models (WWIII and SWAN)

The WWIII version 2.22 and 3.14 was tested in this study. The WWIII is a WAM-type ocean surface wave model developed at NOAA/NCEP (Tolman and Chalikov, 1996 and Tolman, 2002, 2009). It is a further development of the WAVEWATCH I model, developed at the Delft University of Technology (Tolman 1989, 1991a) and WAVEWATCH II, developed by NASA at the Goddard Space Flight Center

(e.g., Tolman, 1992). It nevertheless differs from its predecessors in all the important points: the governing equations, the model structure, numerical methods and physical parameterizations (<http://polar.ncep.noaa.gov/waves/wavewatch/wavewatch.shtml>).

WWIII has been successfully applied in global and regional-scale studies in many areas in the world's oceans, including the North Atlantic (Tolman, 1999, 2002d; Wingert et al., 2001, Guillaume et al., 2010; Rasche and Arduin, in press). It has proven to be an effective tool for studying wave spectral evaluation, air–sea interactions and nonlinear wave–wave interactions.

Like most third-generation wave models that consider current effects, the WWIII solves the spectral balance equation of wave energy in terms of the wave action density spectrum  $N(k, \theta, x, t)$  (wavenumber-based). The implicit assumption in this equation is that the properties of the medium (water depth and currents) vary as the mean-field wave varies in spatial and temporal scales, which are much higher than the scales of variation of a single wavelength (Tolman, 2002, 2009).

Like WWIII, the shallow water model SWAN (Ris et al., 1994; Ris et al., 1999; Booij et al., 1996; Booij et al., 1999; Holthuijsen and Booij, 2003; Booij, 2004) resolves the spectral balance equation in the Cartesian system or spherical coordinates as a function of action density spectrum  $N(x, t, \sigma, \theta)$  (relative frequency-based). The physics of SWAN are different from those of WWIII, especially for shallow water environments. SWAN can simulate shoaling due to spatial variations at the bottom and in the current. It can also simulate refraction, bottom friction, depth-induced wave breaking and the three-wave interactions, which are very important factors for shallow waters.

In the WWIII (2.22 version) sources and sinks correspond to energy transfer between wind and waves ( $S_{in}$ ) (Wind–wave interaction), energy transfer between wave components for deep waters ( $S_{nl}$ ) (nonlinear wave–wave interactions - quadruplets), the dissipation of energy associated with the wave breaking in deep water ( $S_{ds,w}$ ) (denoted as ‘Whitecapping’), and the dissipation of energy related with bottom friction ( $S_{ds,b}$ ). In the new 3.14 version of WWIII, the source terms of depth-induced breaking in shallow waters, ( $S_{db}$ ), and reflection effects, ( $S_{sc}$ ), WAM 4 input and dissipation and bottom scattering are included (Kreisel, 1949; Arduin and Magne, 2007).

Montoya and Osorio (2007) presented a detailed comparison between the most popular ocean wind wave models (including several versions of WWIII and SWAN). As with the versions of the WWIII model, there are important differences between both models related to the physical structure, numerical methods and physical parameterizations, which are not mentioned above. Among the most important differences, the following was highlighted:

*Numerical scheme:* SWAN: Implicit, better behavior for shallow waters than explicit schemes, less efficient for deep waters (first order upwind scheme in geographical space, accurate for near-shore applications, higher order upwind scheme for oceanic scales). WWIII (2.22 and 3.14): Explicit, semi-implicit for source terms, better behavior for deep waters.

*Grids:* SWAN: Arbitrary number of static grids, possibility of unstructured grids. WWIII: Arbitrary number of grid statics and movable, unstructured grids – not yet available (3.14, this allows for moving the grid modeling of hurricanes away from the coast, Tolman and Alves, 2005).

#### 3.3. Hurricane model description

The asymmetric HURWIN hurricane wind model is based on the asymmetric model of Collins and Viehnaman (1971); Jelesnianski (1974) with improvements proposed by Lizano (1990). The wind speed at distance  $r$  is given by  $V(r) = V_{\max}(2Rr/(r^2 + R^2))$  for  $r < R$ , and  $V(r) = V_{\max}(V_{\max}/(C1 r^2)) \text{Log}(R/(C2 r^m))$  for  $r > R$ . Where,  $R$ =radius of maximum wind speed (hereafter  $R_{\max}$ ),  $C1=3.354$ ,

$C_2 = 1.265 \times 10^{-3}$ ,  $k = 0.095$ ,  $m = 1.575$  and  $V_{max}$  is the maximum wind speed around the hurricane eye, estimated using the expression of Collins and Viehnaman (1971). The pressure field in the boundary layer is predefined and fixed. That means that there are not atmospheric gravity waves present in the numerical solution. The wind information is calculated from the available meteorological parameters of historic hurricanes for a specific category. Pressure fields are specified using several models, like those of Holland (1980) and Cardone et al. (1994). The  $R_{max}$  is obtained using the Willoughby (2004) model, given by

$$R_{max} = 46.29 \exp(-0.0153 V_{max} + 0.016 \phi),$$

where  $\phi$  is the latitude,  $V_{max}$  is the maximum 1-min surface wind speed in m/s.

3.4. Blended wind fields (hereafter HURNARR)

Spatial distribution of surface winds during Hurricane Katrina, used as input data for the wave models, was obtained employing the methodology presented by Montoya et al., [Comparison of

several reanalysis data sets combined with the hurricane wind model HURWIN: Methodology to improve wind field during hurricane conditions. Manuscript in preparation]. The methodology combines the next skills inherent in both, reanalysis data sets and the hurricane wind models:

- Reanalysis data sets: Appropriate fit for moderate winds (< 20 m/s) and distant points from the hurricane track for main reanalysis data sets, when compared to in-situ buoy data. Historical information from different databases shows several problems for values near the hurricane eye, mainly due to: (a) Wind data used in the data assimilation process varying with time and space, (b) Problems with wind information from satellite data used in the latest databases such as NARR and JAR for strong and light winds, (c) Poor spatial and temporal resolution of most data sources that do not allow the physics of the phenomenon in the vicinity of the hurricane eye to be captured accurately (asymmetry,  $R_{max}$ , eye location).

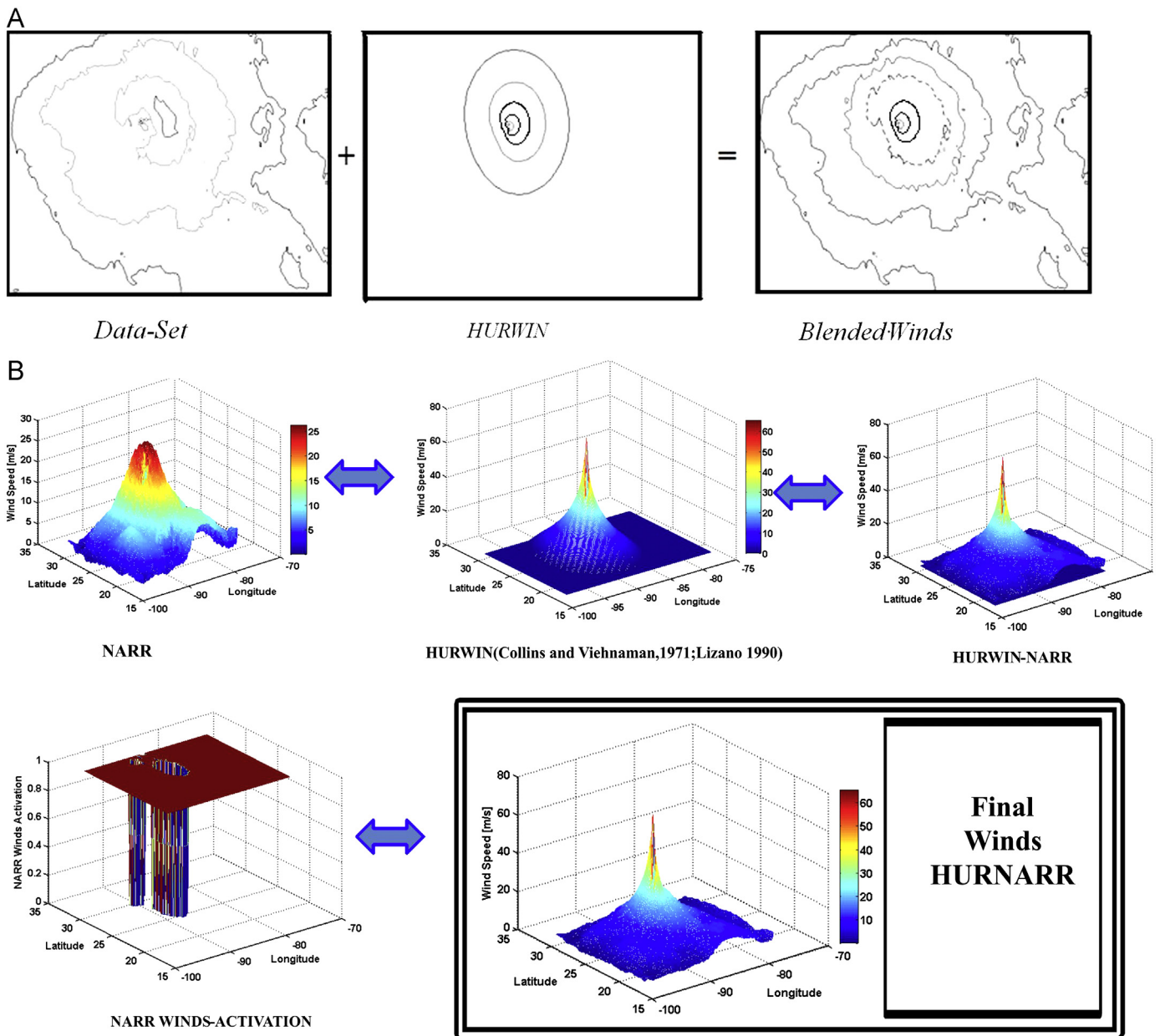


Fig. 2. Blended wind methodology. (A) Schematic methodology showing the blended winds from NARR and HURWIN model in space domain, (B) Application case: Hurricane Katrina and NARR data employed showing environmental winds.

- Hurricane wind models: These provide a more accurate representation of wind fields near the hurricane eye for these parameters.

A description of the methodology is shown below.

- Environmental winds from existing databases were necessary (NARR data for this research). To interpolate them to a spatial resolution equal to that of the hurricane model (depending on mesh size and spatial resolution). To achieve this, the bilinear interpolation method and a temporal resolution of six hours based on track information (pressure, Maximum wind Speed, latitude, longitude), available at <http://www.nhc.noaa.gov> was employed.
- The wind field from the hurricane wind model HURWIN had to be estimated. To accomplish this, first the  $R_{max}$  and the mean constant environmental pressure needed to be obtained. Therefore, the Willoughby (2004) parameterization was employed for  $R_{max}$  and the environmental pressure was obtained from the NOAA North American Regional Reanalysis project (NARR) and the methodology proposed by Veerasamy (2008).
- Surfaces representing the magnitude of wind fields for both sources (environmental wind from the NARR data set and the HURWIN model) using the zonal and meridional wind components (U10 and V10) were calculated.
- The Maximum Envelope Surface (MES) was then estimated. This corresponds to the surface that represents the maximum wind field at each point in space domain. The result is a surface with wind activation obtained from the hurricane model near the eye of the hurricane, and activation of environmental winds from reanalysis data set (NARR) far from the hurricane eye outside of the hurricane environment.

- A filter to avoid environmental wind activation near the hurricane eye (where the hurricane wind model was assumed more appropriate) was applied.
- The positions of the hurricane eye were obtained using the information available at <http://www.nhc.noaa.gov>. To avoid possible distortions to the wind field and hurricane eye position, corrections to the location of the eye for the NARR data set were not applied.

In Fig. 2A the schematic procedure is shown and Fig. 2B shows its application to hurricane Katrina on August 28 2005 12UTC, when the hurricane reached category five.

To address the sources of uncertainties in the proposed blended wind methodology validation, particularly highlighting the sparsity of spatial In-situ buoy wind data, Fig. 3 shows the wind speed from hurricane Katrina for two different dates: at 06:00 UTC on August 28th when Katrina reached category five in the central Gulf of Mexico, and at 06:00 UTC on August 29th when the storm weakened to a category 3 hurricane before making landfall near the Louisiana–Mississippi border at 11:00 UTC on the same day. The results from HURNARR (blended winds) are compared to the Hurricane Research Division (HRD) wind speeds. The HRD analysis uses all available surface weather observations (e.g., ships, buoys, coastal platforms, surface aviation reports, reconnaissance aircraft, Doppler radar and satellite data adjusted to the surface) for obtain the most accurate wind speeds (Powell et al.,1998; Powell et al., 2009; Powell et al., 2010).

The results show that blended winds from HURNARR and HRD winds behave in a similar way. Since winds from HURNARR are a little more asymmetric and exhibit a more rapid reduction of the

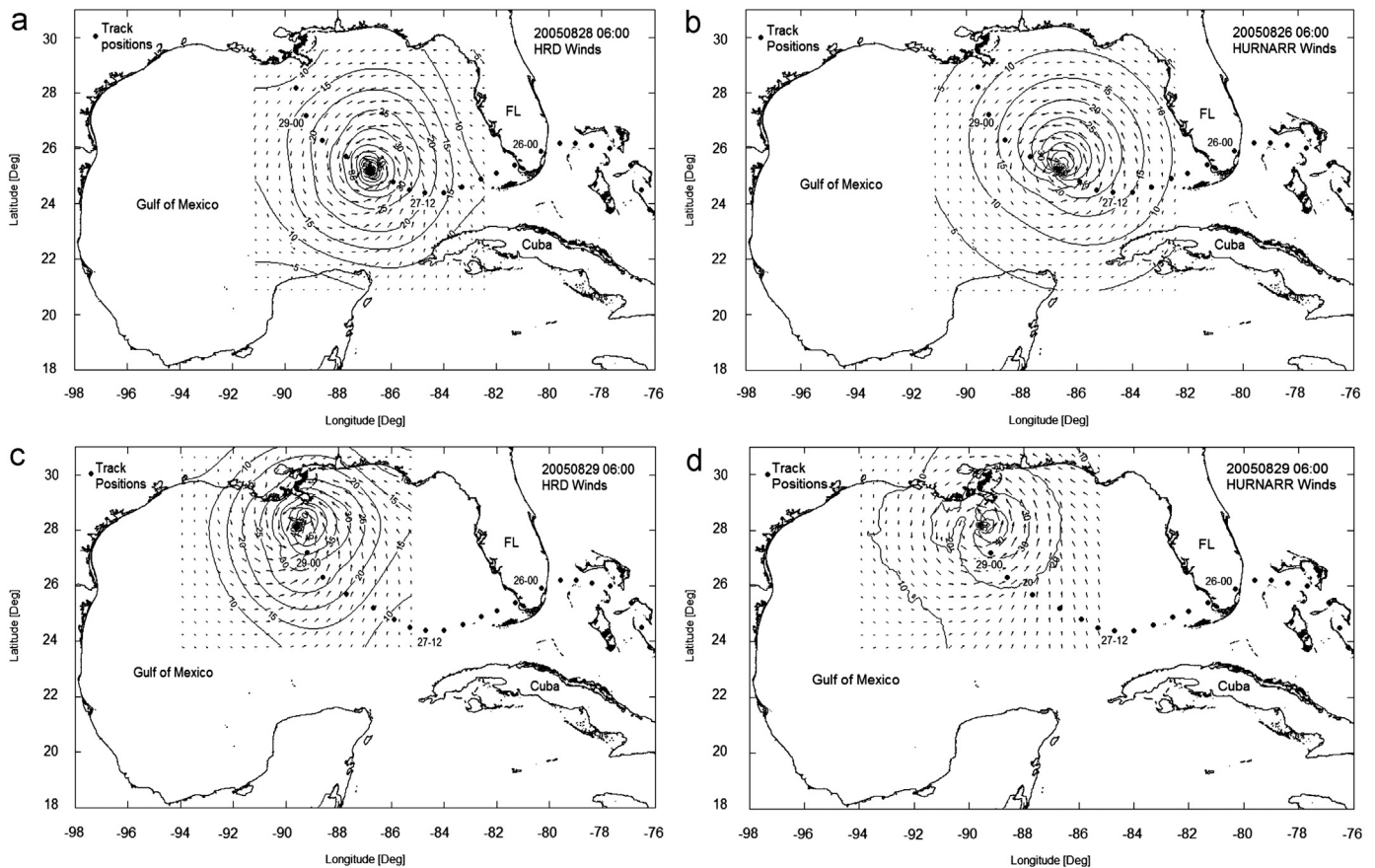


**Fig. 3.** Spatial wind speed comparison for HURNARR and HRD for Hurricane Katrina (m/s). At top 06:00 UTC 28 August and bottom 06:00 UTC 29 August. (a) Wind speed from HRD for 06:00 UTC 28 August, (b) Wind speed from HURNARR for 06:00 UTC 28 August, (c) Wind speed from HRD for 06:00 UTC 29 August, (d) Wind speed from HURNARR for 06:00 UTC 29 August.

magnitude of wind speed with respect to the distance from the eye of the hurricane, their magnitude is well reproduced. Maximum winds of about 55.85 m/s were seen for HURNARR compared to 57.42 m/s for HRD at 06:00UTC on August 28th, and 58.1 m/s for HURNARR and 54.56 m/s for HRD at 06:00 UTC on August 29th.

Several blending techniques have been published previously by various authors, with the aim of obtaining the most accurate possible wind speeds during hurricanes conditions such as Swail and Cox (2000); Chao and Tolman (2001); Zhang et al. (2006); Liu et al. (2007); Stockdon et al. (2007) among others; however the most important advantages of the proposed methodology of Montoya et al. [In preparation:] are its simplicity and applicability for long-term analysis where other methodologies do not have the required information or the results obtained are not of the same spatial and temporal quality. The blended wind quality is directly related to the quality of the reanalysis data set for analyzing environmental winds and the hurricane wind model employed.

#### 4. SWAN and WWIII comparisons

As mentioned above, several papers have been studied the effects of the reduction of the drag coefficient and friction velocity during high wind speed. In the most recent versions of the WWIII model (3.14 and 4.0), a new parameterization was included, referred to as WAM4 and Variants. The evidence of the threshold behavior of the wave breaking process, the underestimation of swell dissipation (Tolman, 2002f), the very strong dissipation at high frequencies given by the dissipation term in the original WAM4 parameterization, and the deficiencies of WAM4 and BAJ source terms in the presence of swell, has lead to several new parameterizations (Tolman, 2009). The best overall parameterization found so far is described by Ardhuin et al. (2008) (Tolman, 2009), and is referred to as "ACC350". For this parameterization (3.14, WAM4 and Variants), an optional ad hoc reduction of friction velocity ( $u^*$ ) is implemented in order to allow a balance with a saturation-based dissipation. This correction also reduces the drag coefficient at high winds.

Based on the above, comparisons were carried out between the available parameterizations in the multigrid version (3.14) of WWIII. The parameterizations were: the BAJ parameterization from Bidlot et al. (2005), the WAM4 parameterization from Gunther et al. (1992), the ACC350 parameterization from Ardhuin et al. (2008), and the parameterization of Tolman and Chalikov (1996) (hereafter TC). The comparisons were based on the performance of the basic statistical parameters, the Mean Average Deviation (MAD) and Root Mean Square Error (RMSE), as given by  $MAD = 1/N \sum_{i=1}^N Abs(X_{measured(i)} - X_{calculated(i)})$  and  $RMSE = \sqrt{1/N \sum_{i=1}^N (X_{measured(i)} - X_{calculated(i)})^2}$ , as well as scatter plot parameters, slope of regression line and coefficient of determination.

The spectral resolution applied was 30 frequencies, varying from 0.042 Hz to 0.65 Hz with an  $\sigma_{m+1} = 1.1\sigma_m$  distribution and 36 directions (10 degree resolution). The time steps employed were 900, 900 and 300 s for the Global, Spatial, intra-spectral and source term integration time steps respectively. Grid configurations used  $\Delta x = \Delta y = 1/6^\circ$  in a spatial domain between  $76^\circ W$  and  $98^\circ W$  and  $18^\circ N$  and  $31^\circ N$ .

Initially the results obtained from the basic wave parameters of significant wave height ( $H_s$ ) and Peak period ( $T_p$ ) were compared using the parameterization of TC for two options (results not shown here): Limited drag corresponding to the FLX3 optional switch from the user manual and with a default value of 2.5E-03 (hereafter TCFLX3). The TC parameterization with the FLX2 option

(Hereafter TCFLX2) without any limitation for the growth of the drag coefficient. The results show a much better performance for significant wave height than for Peak period for the TCFLX2 parameterization. For significant wave height most of the buoys employed (8 buoys, 80%) have lower values of RMSE and MAD due to the widespread underestimation of significant wave height obtained with the TCFLX3 parameterization. The average difference between the buoys with the best results from the TCFLX2 parameterization (8 buoys) is approximately 21% for RMSE and 20% for MAD respect to TCFLX3.

The peak period shows mixed results, for 5 of the 10 buoys (50%) (42003, 42035, 42036, 42039 and 42040) and for 6 of 10 (60%) (42003, 42007, 42035, 42036, 42038, 42039 and 42040) the parameterization of TCFLX2 exhibits better results with lower values of RMSE and MAD respectively. For the other buoys the best results are obtained by TCFLX3. The percentage differences between the best performing buoys for TCFLX2 show very similar results to those obtained for the buoys employing the TCFLX3 parameterization (7.96% and 7.35% for RMSE and 9.59% and 7.21% for MAD respectively). The percentage differences are estimated based on the statistical parameters that have the best results (those with lowest values of RMSE and MAD). Given the above, the peak period does not allow a clear conclusion about the more appropriate parameterization. Thus, underestimates of significant wave height for most of the buoys with the TCFLX3 parameterization, and a better fit for the TCFLX2 parameterization, allow the latter to be selected as the most appropriate for comparison with the WAM4, BAJ and ACC350 parameterizations. The results obtained for significant wave height and Peak period suggest a lesser influence of drag reduction on the estimation of peak period than on that of the estimation of the significant wave height. More research is required to test this behavior.

The comparison of the TCFLX2 parameterization presented the best results when compared to the WAM4, BAJ and ACC350 parameterizations. This can be seen when looking at significant wave height, where it obtained better results for six of the ten buoys (60%) (buoys 42001, 4002, 42003, 42019, 42038 and 42040 with lower values of RMSE and MAD) to than the other three parameterizations. The mean difference respect to TC for all of the six buoys with the best results was 16.43% for MAD and 21.4% for RMSE. Percentage differences vary from 1.4% to 34.8% for MAD and from 1.1% to 57.7% for RMSE, when comparing the TC parameterization against the WAM4. For BAJ the mean percentage difference when compared with the TC parameterization was 24.2% for MAD and 29.9% for RMSE. Values vary between 5.7% and 51.4% for MAD and between 9.6% and 47.3% for RMSE. For ACC350 the mean difference respect to TC for all of the six (6) aforementioned buoys is 57.9% for MAD and 65.2% for RMSE.

Comparisons between the WAM4, BAJ and ACC350 parameterizations for significant wave height showed that although the results for WAM4 and BAJ are very similar (differences are below 10% for 8 out of the 10 buoys), WAM4 performs slightly better. For this parameterization, five out (5) of ten (10) buoys presented lower values (two are equal) for MAD as did five out of ten for RMSE. In all cases the BAJ and WAM parameterizations produced better results than ACC350. This partially contradicts previous results presented by Tolman (2009), who showed that BAJ is generally better than WAM4 and that the ACC350 combination performs better than BAJ in all conditions except for very high waves ( $> 11$  m).

For peak period the results are very similar to those obtained for significant wave height. TC demonstrated better results for five out of the ten buoys (50%) for MAD and seven out of the ten buoys (70%) for RMSE when compared with WAM4, thereby giving the best performance with respect to the TC parameterization. For buoys with best performance for WAM4 parameterization when

compared with the TC parameterization, the statistical parameters (RMSE, MAD) are quite similar. Only for buoy 42001 and when only using RMSE, did the ACC350 parameterization present better results than WAM4, BAJ and TC. The majority of results show that the WAM4, BAJ and ACC350 parameterizations tend to overestimate peak period for higher values.

Employing only the buoys with better results for TC parameterization (five for RMSE and seven for MAD), the percentage differences for peak period were slightly lower. Mean percentage differences of 13.42% for MAD and 8.79% for RMSE were found when compared the WAM4 parameterization against TC parameterization. 16.42% for MAD and 15.93% for RMSE were seen with the BAJ parameterization and 29.14% for MAD and 23.9% for RMSE were observed for the ACC350 parameterization.

Fig. 4 compares the behavior of both parameterizations for the spatial variation in the drag coefficient with respect to Katrina's

geometric structure. It shows the significant wave height and the corresponding drag coefficient for the TC parameterization with and without limited drag (TCFLX2 and TCFLX3 defined above, maximum value of  $2.5E-03$ ) and ACC350 limited drag based on Arduin et al. (2008). A detailed description of the physical behavior of the TCFLX2 parameterization on the effect of surface waves on mature and growing air-sea momentum exchange can be seen in Moon et al. (2004a).

The figure shows relatively similar results in the spatial structure of significant wave height, with higher waves in the right forward quadrant of the hurricane. The effect of using a drag coefficient limited to  $2.5E-3$  for the TCFLX3 parameterization shows an underestimate in the area of maximum winds generated by the reduction in the drag coefficient and thus in the Wind Input term (Sin) (Fig. 4b). Despite the underestimation of significant wave height and large differences in the structure and magnitude

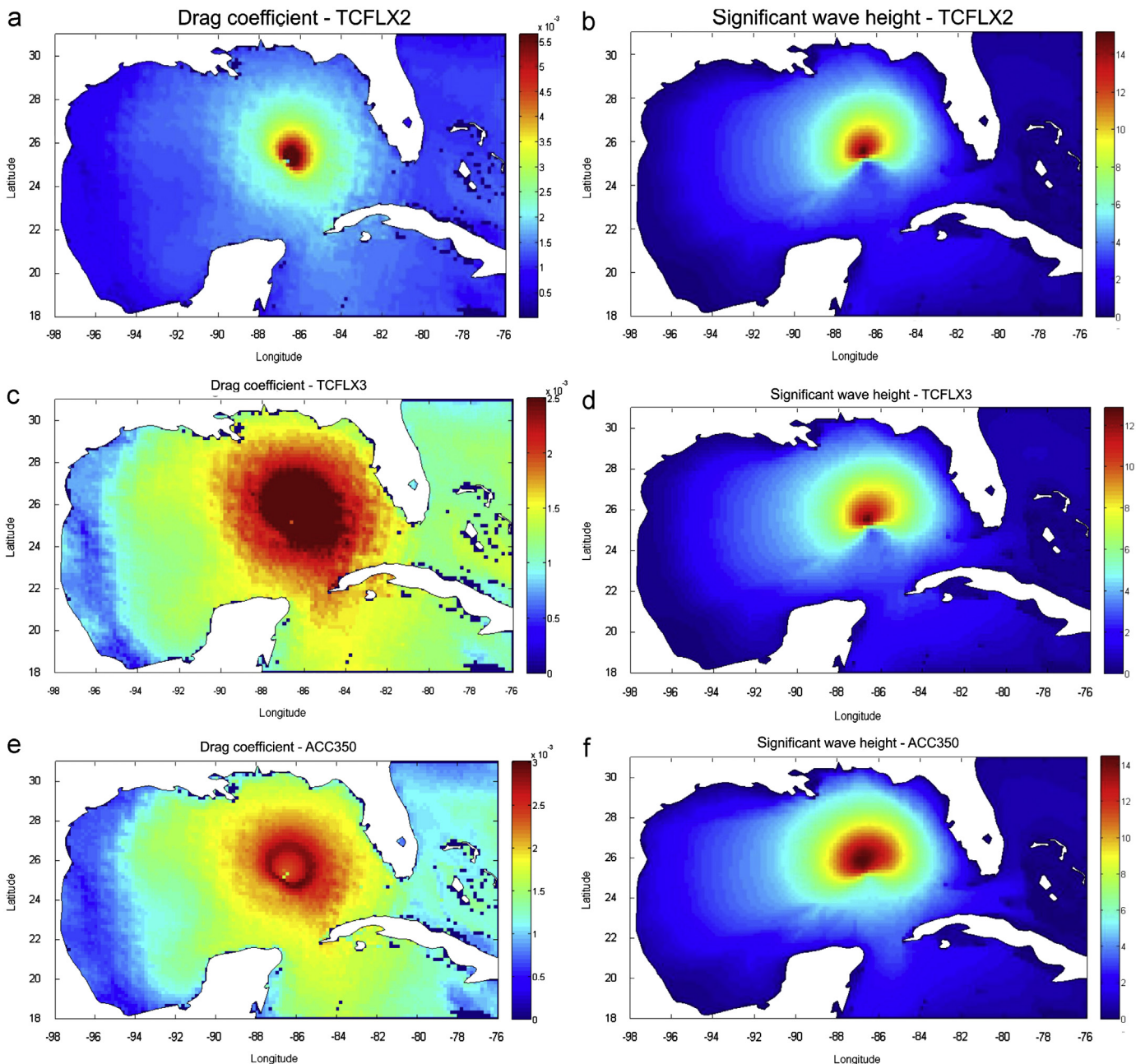


Fig. 4. Comparative results between the TCFLX2, TCFLX3 and ACC350, for 06:00 August 28, 2005. Left figures (a,c,e) represents the spatial behavior of the drag coefficient and the right ones (b,d,f) the spatial behavior of significant wave height (Hs).

of the drag coefficient, the spatial structure of significant wave height for both parameterizations show similar results.

Upon comparing the results of the TCFLX2 parameterization with ACC350, it can be seen that both show very similar values of maximum significant wave height (15.2 m for TCFLX2 and 14.51 m for ACC350). However, as discussed above the ACC350 parameterization tends to have greater values of significant wave height than those presented by TCFLX2 and TCFLX3 for most of the simulation time (results not shown) and most of the buoys. These results may be associated with the spatial structure obtained for ACC350, which tends to show a smaller spatial decrease in significant wave height outside the area of maximum winds possibly induced by the drag limited behavior, thereby generating an apparent overestimation around the eye of the hurricane observed by the In-situ buoys. The difference in significant wave height between the TCFLX2 parameterization and the ACC350 parameterization for the date indicated reaches three meters in regions located in the right forward quadrant where the waves are expected to be more energetic.

Next, in order to make comparisons with the SWAN model, the TC (TCFLX2) parameterization for wind Input (Sin) and dissipation (Whitecapping) (Sds), the Discrete Interaction Approximation (DIA) (Hasselmann et al., 1985) for nonlinear wave–wave interactions, and bottom friction Sds from Hasselmann et al. (1973), were selected. The TC parameterization employs default values (see Tolman, 2002, 2009) which have been tested in tropical zones with very good results by Montoya and Osorio. (2009).

Considering the results presented by Ortiz and Mercado (2008) for the SWAN model, showing the best performance for the exponential wind growth term and dissipation (Whitecapping) (Sds) presented by Komen et al. (1984) from WAM Cycle 3 (WAMDI Group (1988)) when compared with the presented by Janssen (1989,1991a,b), the first one was used, The Discrete Interaction Approximation (DIA) (Hasselmann et al., 1985) for nonlinear wave–wave interactions, and bottom friction (Sds) from Hasselmann et al.(1973) were also employed, similar to the WWIII model. The same spectral resolution as the WWIII model was employed, using 30 frequencies varying from 0.042 Hz to 0.65 Hz with a  $\sigma_{m+1}=1.1\sigma_m$  distribution and 36 directions ( $10^\circ$  resolution). Fig. 5A shows the results obtained for significant wave height (Hs) [m] and Peak period (Tp) [s], for both models and the buoys 42040 and 42003 which were closest to hurricane track in the right forward quadrant, where more energetic waves are expected. Fig. 5B shows the spatial distribution of significant wave height (Hs) for the WWIII model and the wind vectors for 20050828 06:00:00 UTC, when Katrina moved in a general west-northwest direction and reached maximum winds of 63 m/s and a minimum pressure of 930 hPa.

Fig. 5B confirms the results presented by several authors, as discussed above. The highest wind values, wave heights and periods were obtained in the right forward quadrant along the forward motion of the storm, for longer distances than ( $R_{max}$ ). The lowest wave height occurred in the left quadrant of the hurricane.

Table 3 shows the results of the main statistics obtained for all the buoys and for the SWAN and WWIII models. WWIII has better results of the basic statistics for significant wave height and most of the buoys and statistical parameters (7 out of 10 buoys, (70%), 42001, 42002, 42003, 42019, 42036, 42038 and 42040). The exception is the coefficient of determination, for which the SWAN model data shows slightly better results for buoys 42002, 42003 and 42038. However, overall a better spatial representation of significant wave height is produced by the WWIII model; including areas in the upper right front side of the storm track and in general, close to the eye. The mean values of RMSE, MAD, Slope and  $R^2$  for the WWIII model, using all the statistical parameters presented in Table 3, are 0.52 m, 0.36 m, 0.90 and 0.93. These results are better than those obtained by the SWAN model, which

were 0.78 m, 0.51 m, 1.1 and 0.93 respectively. This represents differences in the order of 50.0% and 41.7% in the values of RMSE and MAD respectively.

Only for buoy 42035 both models strongly underestimate the significant wave height, WWIII with error around 61% and SWAN by about 27.5% for maximum values. This may be associated with underestimation of the maximum winds near the location of this buoy, where environmental winds from NARR data were activated during the entire simulation period. Physically, the underestimation of winds may be associated with the way certain coastal topography effects affecting the magnitude and direction of the wind. Such effects would not be reproduced by the atmospheric models given the coarse resolution (Ladd and Bond, 2002; Ruti et al., 2008; Cavaleri and Sclavo, 2006). On the other hand, it could be a result of decreasing wind quality in near shore satellite data employed for assimilation processes in NARR reanalysis data (30–40 km from the coastline), as reported by several authors (Pickett et al., 2003; Perlin et al.,2004; Ruti et al., 2008). Buoys 42035 and 42007 are located at about 30 km from the shoreline (both at 13.7 m of depth) in deep and intermediate waters.

Results for peak period are similar to those obtained for significant wave height. The WWIII model provides better values of the basic statistics that measure the degree of scatter of data, such as the RMSE, MAD, and  $R^2$  and the degree of under-or overestimation of the data corresponding to the slope of the regression line. For most of the buoys (8 out of the 10 employed (80%)), results for WWIII have lower values of RMSE and MAD, higher coefficients of determination  $R^2$  and slope values closer to 1. A general analysis shows that for high values, the SWAN model tends to overestimate the measured peak period for most of the buoys (42007, 42019, 42035, 42038 and 42040).

The largest discrepancies are observed for buoys 42001 and 42019, where the basic statistics show contradictory results as to which model best represents the peak period. Buoy 42001 has a slightly lower value of RMSE and the highest value of  $R^2$  for SWAN model, indicating less scatter of the data. In contrast, the WWIII model presents a lower value of MAD and a slope value closer to 1 (minor underestimation or overestimation). Mean values for the basic statistics of RMSE, MAD, slope and  $R^2$  are approximately 2.28 s, 1.69 s, 1.02 and 0.74 respectively for WWIII and 2.82 s, 2.3 s, 1.17 and 0.72 respectively for the SWAN model (differences of approximately 23.68% and 36.1% for RMSE and MAD respectively).

For wave direction, the WWIII model shows better results than those obtained for the SWAN model. When comparing all values in Table 3 (bold text), there are more statistics showing better results for the WWIII model than SWAN (15 statistics for WWIII against 3 for SWAN). For seven of nine buoys (77.85%) the WWIII shows lower values of RMSE and MAD. Mean values of RMSE and MAD are  $41.7^\circ$  and  $30.1^\circ$  for WWIII, and  $56.3^\circ$  and  $38.5^\circ$  for the SWAN model.

Peak periods obtained from the SWAN model tend to overestimate the measured data when all the values are considered. This is verified when observing the slope value obtained from the scatter plots (results not shown here) and Table 3. For the SWAN model, only buoy 42036 has a value of less than 1 (underestimation). The percentage of overestimation (Table 3 slope values) varies from 2% for buoy 42035 and 45% for buoy 42040 with a mean value of 17%. Ortiz and Mercado (2008) employed three buoys located far from the east coast of the United States to compare the time series over two months (June 1–July 30) for peak period and significant wave height, looking at both the SWAN and WWIII models. In these months shallow water effects were not present and the same forcing existed as that from winds when tropical storm conditions appear in the North Atlantic basin. They showed that both models tend to underestimate the Maximum values of peak period. Such a situation is only partially confirmed

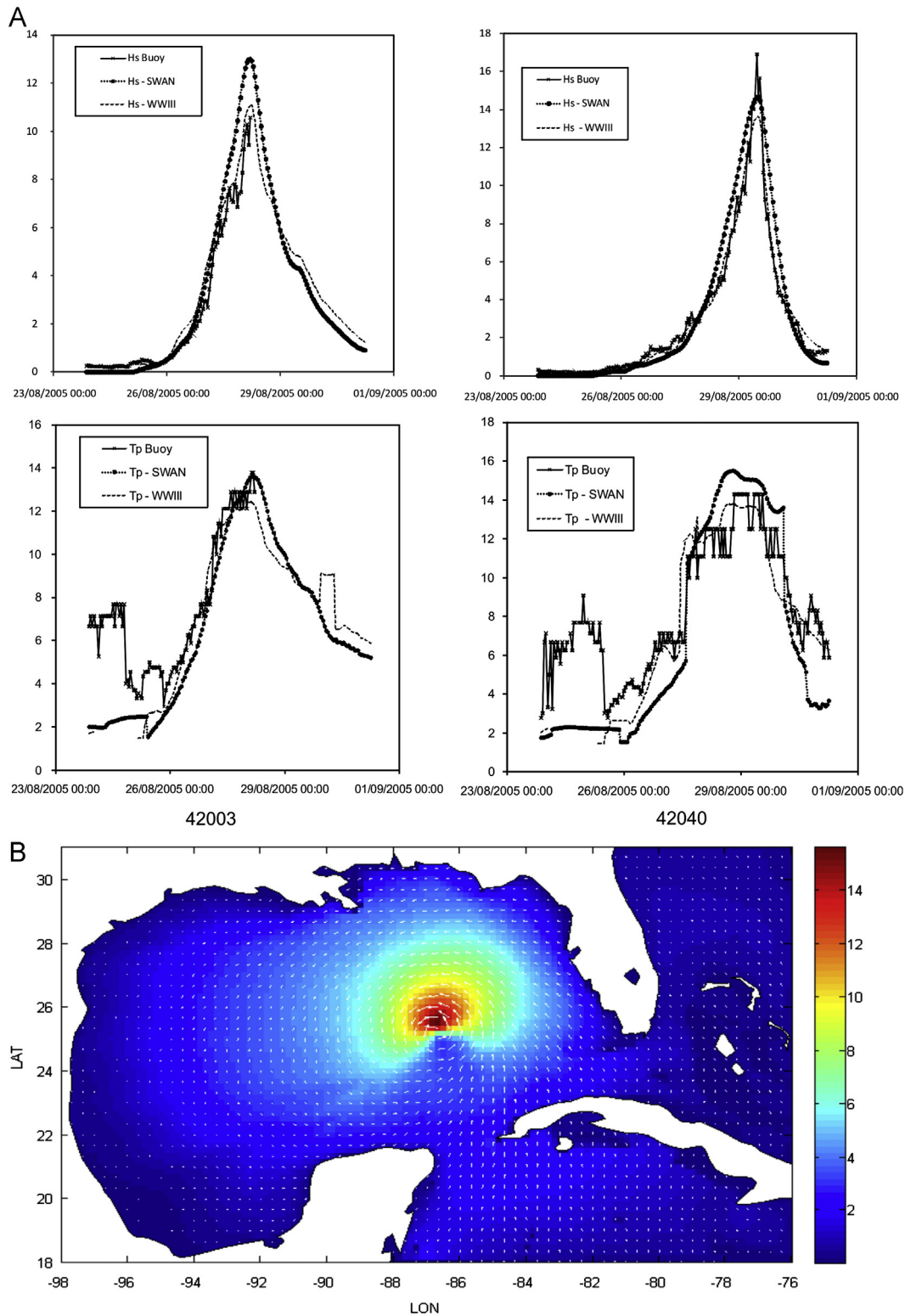


Fig. 5. (A) Peak period (Tp) and Significant wave height (Hs) comparison for the SWAN and WWIII models (nearest buoys in the right forward quadrant 4003 and 42040). (B) Spatial distributions of Significant Wave Height for 20050828 06:00:00 UTC. The Arrow represents the direction of the hurricane translation.

in this study, mainly by WWIII model where some buoys, such as 42003, 42019, 42035, 42036 and 42039, and 42040, underestimate most of the maximum values for peak period. For the SWAN models contradictory results was obtained with five (5) of ten (10) buoys with overestimation of the maximum peak period values (42001, 42007, 42035, 42038 and 42040).

Ortiz and Mercado (2008) confirm that better results are obtained for WWIII than SWAN mainly for significant wave height. This difference is attributed to the way wind energy is transferred to wave energy (Sin) and its dissipation due to whitecapping (Sds) in the models. Wind input parameterization in WWIII (Tolman and Chalikov, 1996) shows a better response to relatively fast changes

**Table 3**  
Wave statistics for the SWAN and WAVEWATCH III models for all the buoys employed.

Buoy	Model	Wave parameter								MWD (Dirp)	
		Hs				Tp				RMSE	MAD
		RMSE	MAD	SLOPE	R <sup>2</sup>	RMSE	MAD	SLOPE	R <sup>2</sup>		
42001	WWIII	<b>0.55</b>	<b>0.39</b>	<b>1.00</b>	<b>0.94</b>	2.36	<b>1.78</b>	<b>0.99</b>	0.72	<b>63.82</b>	<b>47.0</b>
	SWAN	1.36	0.81	1.49	0.94	<b>2.26</b>	1.79	1.25	<b>0.81</b>	75.25	58.64
42002	WWIII	<b>0.69</b>	<b>0.48</b>	<b>1.01</b>	0.64	<b>3.57</b>	<b>2.58</b>	<b>0.92</b>	0.41	54.74	33.81
	SWAN	0.85	0.50	1.42	<b>0.74</b>	3.70	2.79	1.13	<b>0.44</b>	<b>50.64</b>	<b>33.29</b>
42003	WWIII	<b>0.58</b>	<b>0.43</b>	<b>1.11</b>	0.98	<b>1.19</b>	<b>0.93</b>	<b>1.09</b>	0.95	<b>24.58</b>	<b>19.11</b>
	SWAN	1.14	0.67	1.32	<b>0.99</b>	1.47	1.25	1.16	<b>0.97</b>	48.81	29.31
42007	WWIII	0.71	0.53	<b>0.70</b>	0.95	<b>1.49</b>	<b>1.16</b>	<b>1.10</b>	0.91	<b>21.42</b>	<b>17.35</b>
	SWAN	<b>0.69</b>	<b>0.51</b>	0.68	<b>0.97</b>	1.91	1.62	1.28	<b>0.94</b>	56.28	35.66
42019	WWIII	<b>0.23</b>	<b>0.17</b>	0.93	<b>0.95</b>	<b>3.70</b>	<b>2.58</b>	0.83	0.39	<b>46.48</b>	<b>30.21</b>
	SWAN	0.27	0.21	<b>0.99</b>	0.93	4.32	3.56	<b>1.04</b>	<b>0.41</b>	56.28	35.66
42035	WWIII	0.56	0.35	0.40	<b>0.95</b>	<b>3.25</b>	<b>2.46</b>	<b>0.98</b>	0.63	<b>48.31</b>	<b>39.07</b>
	SWAN	<b>0.29</b>	<b>0.21</b>	<b>0.80</b>	0.88	4.71	3.89	1.02	<b>0.39</b>	58.08	46.02
42036	WWIII	<b>0.38</b>	<b>0.29</b>	<b>0.96</b>	<b>0.95</b>	<b>1.09</b>	<b>0.85</b>	<b>0.94</b>	0.90	<b>60.79</b>	46.79
	SWAN	0.59	0.44	0.86	0.94	2.31	2.01	0.74	0.87	62.78	<b>46.30</b>
42038	WWIII	<b>0.38</b>	<b>0.25</b>	<b>0.94</b>	0.97	<b>2.60</b>	<b>1.96</b>	<b>1.06</b>	0.76	Nd	Nd
	SWAN	0.92	0.54	1.40	<b>0.98</b>	<b>2.76</b>	2.11	1.28	<b>0.80</b>	<b>Nd</b>	<b>Nd</b>
42039	WWIII	<b>0.57</b>	<b>0.40</b>	<b>0.97</b>	0.95	1.94	<b>1.38</b>	<b>1.16</b>	<b>0.85</b>	<b>20.99</b>	<b>14.07</b>
	SWAN	0.62	0.48	0.92	<b>0.96</b>	<b>2.31</b>	1.93	1.21	0.84	42.25	24.08
42040	WWIII	<b>0.52</b>	<b>0.34</b>	<b>0.97</b>	<b>0.98</b>	1.64	<b>1.22</b>	<b>1.09</b>	<b>0.85</b>	<b>34.52</b>	<b>23.54</b>
	SWAN	1.10	0.71	1.15	0.96	<b>2.40</b>	2.08	1.45	<b>0.85</b>	56.35	37.59

Nd=No data for specific buoy. Bold text corresponds to best fit for the specific parameter. For RMSE and MAD calculations the wind direction was corrected when the difference between two values was greater than 180°.

in wind speed than the parameterization of Komen et al. (1984) used in SWAN. Despite the WWIII model performs better than the SWAN model for most of the simulation period, it underestimates the significant wave height at the peak of the hurricane as has been showed by several authors.

#### 4.1. Directional and frequency wave spectrum

As discussed above there are several methods to obtain the directional spectrum using the first few Fourier harmonic terms only. NDBC buoy measurements provide enough information for deriving the first 2 Fourier harmonics terms. Apparently this approximation may have its limitation but this is limited by buoy's heave-pitch-roll data. Data-adaptative schemes such as MLM and MEM may give a higher resolution direction distribution but there is not direct link to improved accuracy. Some directional results by MEM and MLM may be numerical artifacts and may not be real, [David Wang, personal communication. Oceanography Division, Naval Research Laboratory, Stennis Space Center Mississippi, Nov 16, 2011] for that reason the method provided by Longuet-Higgins et al. (1963) was employed in this research. Given the possible distortions involved in the directional spreading functions estimation according to the method employed, the frequency spectrum is also discussed. To compare the directional wave spectrum and the frequency wave spectrum from the WWIII and SWAN models against in-situ buoy data relating to quadrant location in the storm track, the following cases and buoys were selected.

**Case 1.** This case involves directional wave spectrum for buoy 42003, from 20050827 12:00 UTC to 20050828 05:00 UTC, each six hours approximately. During the occurrence of Katrina, data from buoy 42003 was available only for the period from 20050823 21:00 UTC to 20050828 05:00 UTC. In this case it is discussed the influence of relative position (decreasing distance over the time) respect to the eye of the hurricane for a point located in the right forward and backward quadrant, respect to the direction of hurricane translation (north-westward). For this quadrant the more energetic waves are expected and the temporal evolution

of wave growth behavior is fundamental for research and engineering applications.

**Case 2.** For this case, directional wave spectrum for buoy 42003 was analyzed during initial wave growth conditions (young seas). On 20050826 00:00 UTC buoy 42003 was located at approximately 528 km from the eye of the hurricane outside of the hurricane environment where the winds are weaker (distant buoy-only NARR winds are activated near the buoy location).

**Case 3.** Finally, directional wave spectrum was investigated for buoy 42001 on 20050829 12:00 UTC, when the buoy was located in the left forward quadrant with respect to the direction of hurricane translation. Here a more complex structure is normally displayed with both swell and wind wave peaks (Zhuo et al., 2008; Moon et al. (2003)).

For all tested cases; distance from the eye of the hurricane is greater than  $R_{max}$ , obtained with the expression presented by Willoughby (2004).

Figs. 6A, 8A and 10A, show the locations and distances (R1 and R2) of the buoys 42001 and 42003 relative to the center of the hurricane eye and the Figs. 6B, 8B and 10B the directional wave spectrum for all the cases mentioned above. Plots were made employing several frequency limit values based on the location of the main energy inside the spectrum. On the middle right of the figure, main wave parameters are shown: peak period (Tp) [s], peak frequency (fp) [Hz], and peak direction (Dirp) [Degrees]. At the bottom, significant wave height (Hs) and wind parameters such as wind direction (WD) [Degrees] and wind speed (WSPD) [m/s] are also shown. For all cases, in part A of the figures the arrow represents the direction of hurricane translation and R represents ( $R_{max}$ ). The scale bar on the right side represents the wave spectral energy in  $m^2s^{-1}$ .

Case 1 (Fig. 6): This figure shows the evolution of the directional spectrum every 6 h for buoy 42003 from 20050827 12:00 UTC to 20050828 05:00 UTC (The latter date corresponds to the closest location of buoy 42003 from to the eye of the hurricane, according to the available information). For the former date (20050827 12:00 UTC), buoy 42003 is located on the right forward quadrant with a

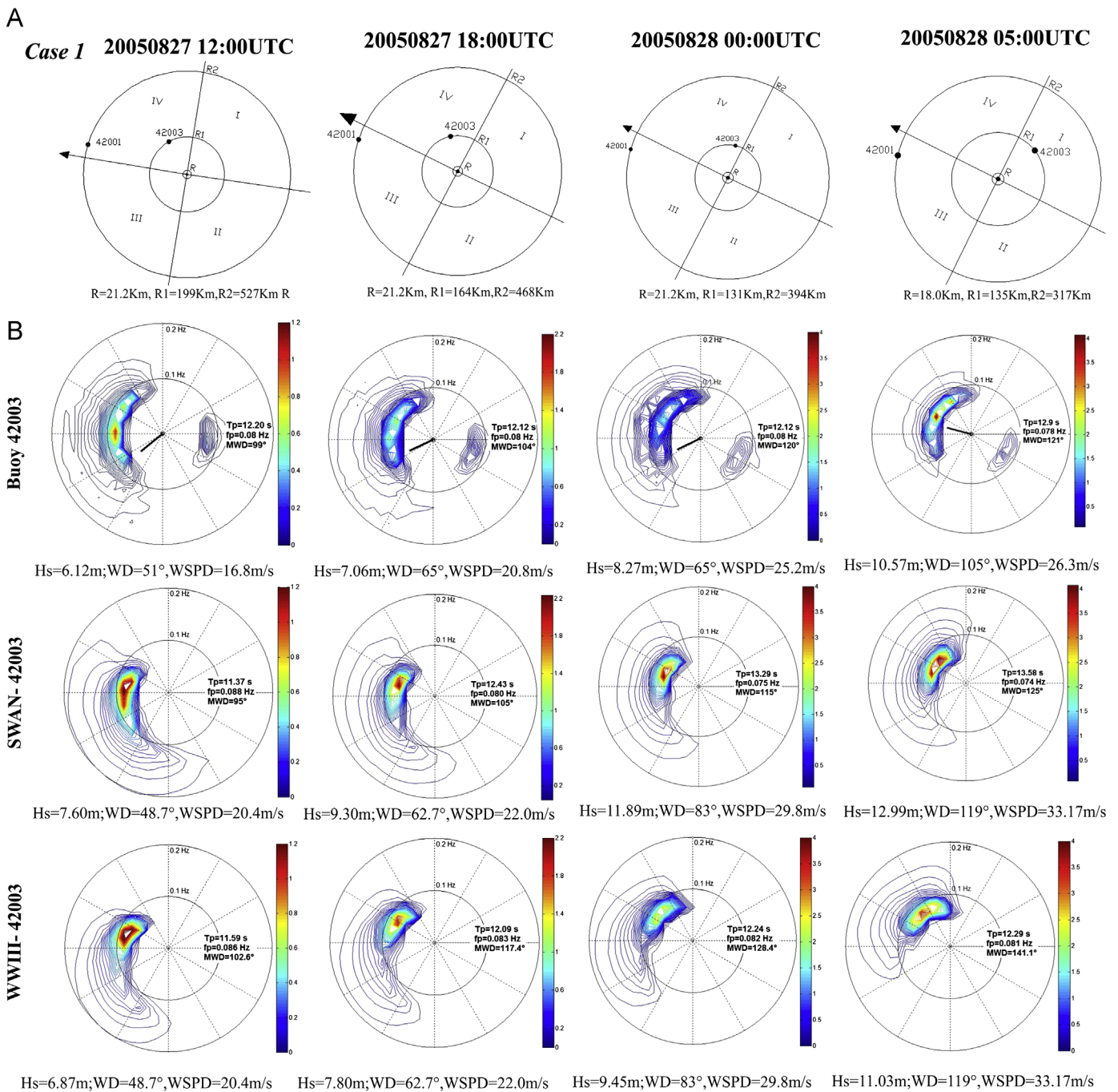


**Fig. 6.** (A) Location of the buoys 42003 and 42001 relative to the eye of the hurricane, (B) Comparison between directional wave spectrum from NOAA buoy 42003 and WWIII and SWAN models for several dates and buoy location.

distance from the eye of the hurricane, of approximately 199 km (R1) and 69.2° right of the direction of hurricane translation. Buoy 42003 has two predominant components of energy (bimodal) for this date: one westward propagating in the direction of the hurricane translation (usually expected in such conditions (Walsh et al., 2001; Moon et al., 2003; Zhuo et al., 2008) and another in the opposite direction, not reproduced by WWIII or SWAN models (approximately eastward). The aforementioned seems to correspond to an anomalous component, which is not expected for this quadrant based on the location and distance of the buoy relative to the eye of the hurricane.

For the aforementioned date both, the SWAN and WWIII models show similar results for the shape of the spectrum but

with more energy concentrated around the spectral peak and slightly worse directional distribution of the spectrum for the SWAN model. Both models show very similar results for peak period and peak frequency (differences less than 7%), but the WWIII model reproduces in better way the peak direction (MWD-Dirp) with a single error of 3.6%, slightly lower than the SWAN model which gave 4.04%. For this quadrant both models adequately reproduce a unimodal swell system with lower peak frequencies propagating in the direction of hurricane translation. Less dispersion and high-energy concentrated around the spectral peak frequency (less energy for higher frequencies > 0.2 Hz) can be observed, as well as high gradients of energy around the spectral peak.

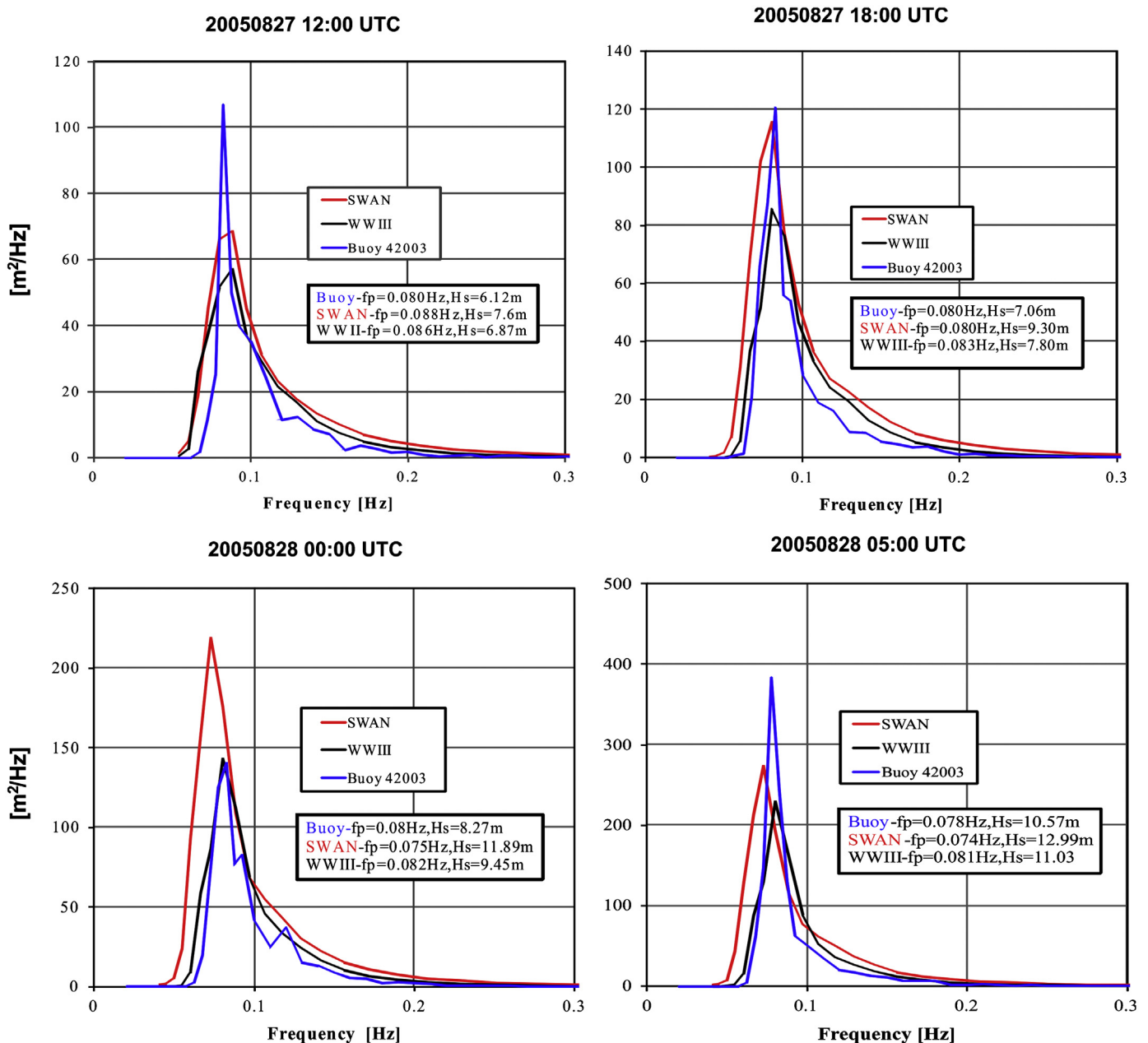


**Fig. 7.** Measured and predicted frequency spectrum for selected dates and buoy 42003 for Case 1. Dates selected correspond to the nearest distances between the eye of the hurricane and buoy location.

For significant wave height, on 20050827 at 12:00 UTC, the location of buoy 42003 in the right forward quadrant and its smaller distance from the eye of the hurricane were reflected in the results of significant wave height (highest values), 6.12 m for the buoy, 7.6 m (24% error) for SWAN and 6.87 m (12.2% error) for WWIII. Such results show the overestimation of significant wave height by the SWAN model, as shown in Fig. 5. Six hours later (20050827 18:00 UTC) when the hurricane was moving at a speed of approximately 3.22 m/s and reached Category 3 in the north-west direction, buoy 42003 remained in the right forward quadrant at a closer distance relative to the eye of the hurricane about 164 km and 61.4° from the direction of hurricane translation (see Fig. 6A).

The maximum significant wave height reached 18 m in the right forward quadrant of the hurricane near the eye and it propagated in the same direction as the hurricane. During hurricane conditions, waves to the right and front of the hurricane are

exposed to prolonged forcing from strong winds. Such forcing results in the formation of higher and longer waves to the right and front of the track, while lower and shorter waves are formed to the rear and left (Moon et al., 2003; Liu et al., 2007).

Again buoy 42003 shows two components of low frequency (swell) in the westward direction to the left of the direction of hurricane translation, as well as a component of low frequency energy traveling eastward. The first component presents a unimodal directional spectrum with a narrower spread and low peak frequency ( $< 0.1$  Hz), moving in the direction of hurricane translation (Walsh et al., 2001; Moon et al., 2003; Zhuo et al., 2008). The eastward system does not seem reasonable. This situation is repeated for the directional spectrum obtained by buoy 42003 for the other dates shown in Fig. 6B (20050828 00 UTC and 20050828 05:00 UTC). The latter date corresponds to the closest location of buoy 42003 from the hurricane track, according to the available information.

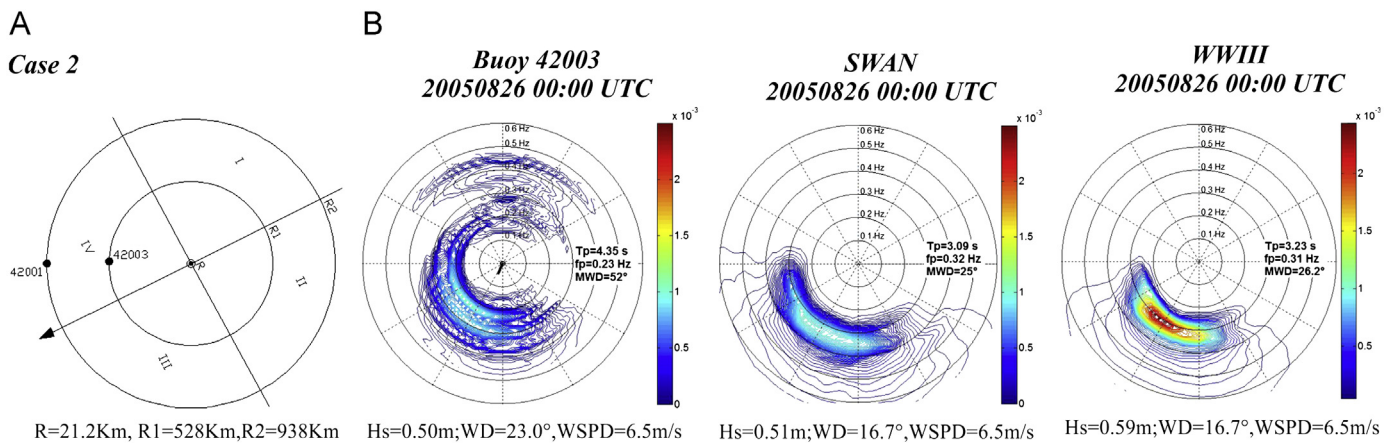


Fig. 8. (A) Location of the buoys 42003 and 42001 relative to the eye of the hurricane, (B) Comparison between directional wave spectrum from NOAA buoy 42003 and WWIII and SWAN models for Case 2.

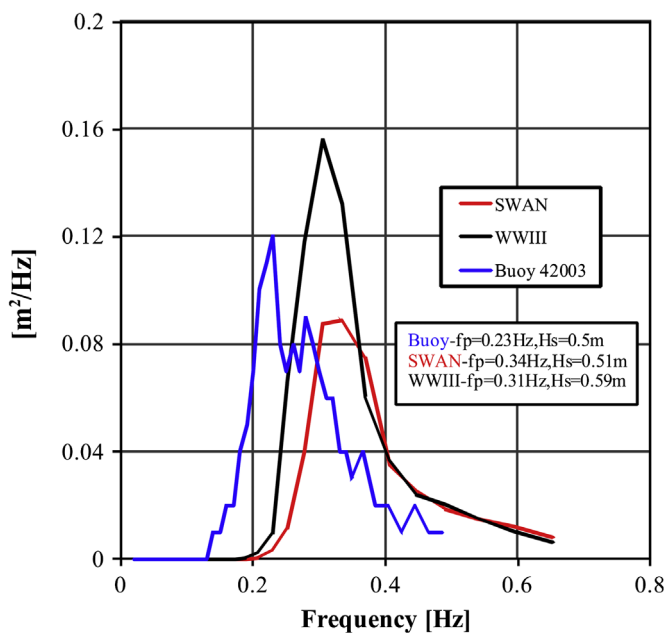


Fig. 9. Measured and predicted frequency spectrum for buoy 42003, low sea states-Case 2. During 20050826 00:00 UTC.

For 20050827 at 18:00 UTC again the WWIII model slightly better reproduces higher-energy areas concentrated around the spectral peak as well as the asymmetry of low frequencies in the southwest part of the spectrum. The peak period and peak frequency are adequately reproduced by both models for the last three dates, with very similar results. However, the mean percentage error given by the WWIII model estimated using the three dates is slightly lower than the one shown by the SWAN model (1.99% against 5.84%). Higher values for the SWAN model were produced by greater differences, up to 9% for the spectrum obtained on 20050828 at 00:00 UTC.

For the peak wave direction (Dirp, buoy 42003) the WWIII model has larger errors for the last three dates, 12.88%, 7.0% and 16.6% for 20050827 18:00 UTC, 20050828 00:00 UTC, and 20050828 05:00 UTC respectively compared with values obtained for the SWAN model of 0.96%, 4.2% and 3.3%. The values obtained by the WWIII model tend to be higher, with dominant energy eastward. For values of significant wave height, the WWIII model shows much better agreement with values measured by the buoy while the SWAN model tends to overestimate the values (by up to

25% for 28th August 05:00 UTC), which verifies the information shown in Fig. 5.

The WWIII model slightly better represents the directional distribution of energy in a northeasterly direction. This is shown by the buoy being in the direction of hurricane translation (narrower spread). However, the WWIII model tends to over-estimate the wave direction associated with the spectral peak, showing values further east (higher Dirp). The WWIII model shows the best results for significant wave height for all simulation periods.

For case 1, both models adequately reproduce the misalignment of local wind and waves and dominant waves located to the right of the wind direction. This is a common spectral characteristic observed in buoy data and other sources of data, for instance that from the Scanning Radar Altimeter (SAR). Several authors, such as Moon et al. (2003); Zhuo et al. (2008), have shown that the deviation between the wind and waves should increase with distance from  $R_{max}$ . This behavior is well represented by both the WWIII and SWAN models, with the best agreement for SWAN (angles between the waves and winds of  $46^\circ$ ,  $42^\circ$  and  $32^\circ$  for distances of 199, 164 and 131 km against  $53.9^\circ$ ,  $54.3^\circ$  and  $45.4^\circ$  for the same distances). Despite these results, the expression presented by Moon et al. (2003) as a function of  $R_{max}$  and distance from the hurricane center is not well represented by either models or even by the buoy data. On the contrary, the potential expression presented by Zhuo et al. (2008) gives the best results for both models. Fig. 7 shows the frequency spectrum for the WWIII and SWAN models against the buoy data for the buoy 42003.

The results for the frequency spectrum show that both SWAN and WWIII models adequately reproduce the growth of the energy spectrum and its shift to lower frequencies (decrease in the peak frequency). This is consistent with the position of the buoys respect to the location of the eye of the hurricane and the area of maximum winds for the four dates analyzed. The distances from the eye for 42003 were 199 km (20050827 12:00 UTC), 164 km (20050827 18:00 UTC), 131 km (20050828 00:00 UTC) and 135 km (20050828 05:00 UTC) in the right forward quadrant of the hurricane with more energetic winds and waves for the first three dates.

Both models reproduce the peak frequencies in a very similar way with slightly better results for the WWIII, as discussed above. The SWAN model tends to be slightly worse at reproducing peak frequency than WWIII for the last two dates.

For most of the dates, the SWAN model tends to have lower values of peak frequency, a greater spectral energy content and a broader frequency spectrum than WWIII, peak energy values approximately 37% higher for 20050827 12:00 UTC, 35% for

20050827 18:00 UTC, 56% for 20050828 00:00 UTC, and 19% for 20050828 05:00 UTC. The higher energy growth is reflected in the greater values of significant wave height than those measured by the buoy. For buoy 42003 WWIII more adequately reproduces the values of significant wave height and the peak period than SWAN as mentioned above.

According to Bolaños-Sanchez et al. (2007), the increase in spectral power of the SWAN model may be generated by energy overestimation for the high frequencies (energy tail), producing an increase in total energy, and therefore, an increase in significant wave height as well as an underestimation of the mean period. For the results obtained in this study, the spectral energy overestimation for high frequencies (energy tail) in the SWAN model is observed for buoy 42003 for all dates, confirming the results obtained by Bolaños-Sanchez et al. (2007).

For buoy 42003, the two models tend to overestimate the significant wave height, because both show a significant increase in the amount of energy contained in the spectrum when compared with energy measured by the buoys. Since the distance from the buoy location to the eye of the hurricane decreases towards areas with higher winds and more energetic waves for buoys located in the right forward quadrant, both models tend to have a broader spectrum than that obtained by the buoy. The buoy tends to have narrower frequency spectrum with lower a peak period, typical of swell systems. The frequency wave spectrum for buoy 42003 does not have the anomalous peaks observed on the directional spectrum.

**Case 2.** (Fig. 8): On 26 August 2005, when the hurricane Katrina crossed the region of Florida in the United States and reached Category 1, typical conditions of low sea states were observed. In this case both models adequately reproduce most energy in the southwest direction, with a wide spread and directional components of high frequency energy characteristic of wind sea for frequencies higher than 0.2 Hz or 0.15 Hz. In this case buoy 42003 is located at a distance of approximately 528 km from the eye of the hurricane (NARR winds are activated, see Fig. 2). Despite this, both models have problems reproducing the existing energy in the north and northeast direction for frequencies higher than 0.3 Hz. However, this energy component does not seem reasonable given the predominant wind direction before the date of 20050826 00:00 UTC at locations so far to the south, southwest, west and northwest (results not shown here), without predominant winds in the north or northeast.

Both models have very similar results of peak wave direction, peak period and peak frequency, nevertheless, the WWIII model slightly better reproduces the values of peak frequency and peak

period when compared with the buoy data (28.97% error for the SWAN model and 25.74% for WWIII). Both models underestimate the value of peak direction, presenting an area of greater energy to the south, which may be due to differences in the predominant wind direction and field records obtained by NARR reanalysis data. Contrary to the results obtained for most of the cases studied, the SWAN model provides better results than those obtained by the WWIII model for significant wave height ( $H_s$ ) (0.51 m for the SWAN model, 0.59 m for the WWIII model compared to a value of 0.5 m measured at the buoy). This represents an error of 2% for the SWAN model and 18% for the WWIII model.

For more energetic waves (Case 1, buoy 42003 located in the right forward quadrant), the method of Longuet-Higgins et al. (1963), although characterized by strongly increased directional spreading as discussed above, gives results consistent with numerical models, however for weak sea states the method has higher directional spread compared with the results obtained by WWIII and SWAN models (Fig. 8). Fig. 9 shows the frequency spectrum for 20050826 00:00 UTC, representing low sea states for buoy 42003, located in the right forward quadrant.

For wake wave conditions, both models underestimate the peak period and concentrate the energy at higher frequencies than those obtained by the buoy. For this parameter the results obtained by the WWIII model are slightly better than those obtained by the SWAN model, with errors of around 34% and 48% for SWAN and WWIII respectively. Despite this, the SWAN model gives better results for significant wave height (0.51 for SWAN against 0.50 for the buoy, error of 2%). For high frequencies, both models tend to come up with greater energy values than those obtained by the buoys, but with similar spectrum amplitude. In contrast, for values obtained for more energetic waves the models tend to have a broader spectrum. Regarding the maximum energy the two models show contradictory results. While the WWIII model tends to overestimate the peak energy with a difference of 30%, the SWAN model tends to underestimate this energy with an error percentage of approximately 25%.

**Case 3.** (Fig. 10): For the date 20050829 00:00 UTC, buoy 42001 was located in the rear and left of the hurricane approximately  $138^\circ$  from the direction of hurricane translation and 152.6 km from the eye of the hurricane location. For this condition a more complex directional spectrum structure is expected with simultaneous wind sea and swell peaks and a greater spread of energy (Walsh et al., 2001; Moon et al. (2003); Zhuo et al., 2008). This situation is verified by the buoy results that show the formation of different components of energy (peaks). A very low energy component with high frequencies is seen in the eastern direction

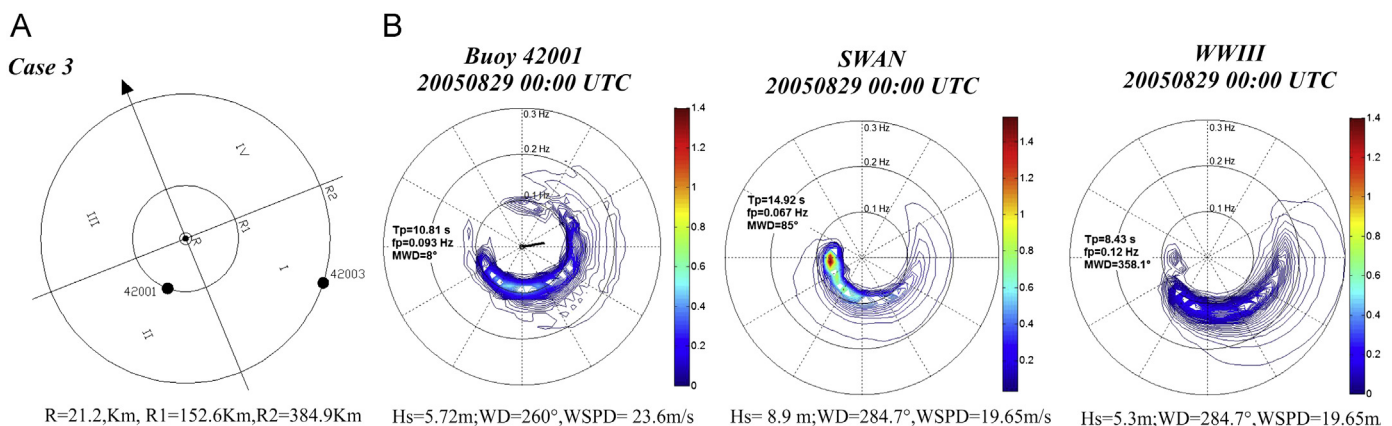


**Fig. 10.** (A) Location of the buoys 42003 and 42001 relative to the eye of the hurricane, (B) Comparison between directional wave spectrum from NOAA buoy 42001 and WWIII and SWAN models for case 3.

(> 0.15 Hz), characteristic of wind seas. Several low-energy spectral components exist in the north and west directions with frequencies of around 0.1 Hz. The higher energy component (main peak) is concentrated at frequencies lower than 0.1 Hz (Swell) with periods of around 10 s in the southwest direction (MWD=8°). Directional spectrum for buoy 42001 presents a wide spread of energy in almost the entire frequency range of the spectrum. The directional spectrum obtained with the SWAN and WWIII models reproduce well the directional spread of energy but have some significant differences that favor one model or the other. The WWIII model generates energy for frequencies close to 0.3 Hz (wave periods of about 3 s and small wavelengths), that are not reproduced by buoy 42001. On the contrary, the SWAN model limits the energy to a value in the order of 0.2 Hz, similar to that obtained for buoy 42001. Despite this, the WWIII model most adequately reproduces a higher concentration of energy (main peak) in the south and southwest with the peak period, peak frequency and peak wave direction closest to values obtained by the buoy.

The SWAN model produces a higher-energy peak in the west direction (right over the value obtained by the buoy) with a higher peak period of 14.97 s compared with 10.81 s reported by the buoy. It also produces a lower peak frequency of 0.066 Hz with respect to 0.093 Hz obtained by the buoy (bigger waves in the area of high energy). These values lead to an overestimation of the significant wave height, giving a reading of 8.9 m compared to a value of 5.72 m measured by the buoy (55% error approximately). The WWIII model by contrast is in strong agreement with the buoy giving a value of 5.3 m (only a 7.3% error), which is much lower than that obtained by the SWAN model. The WWIII model reproduces the energy component in a westerly direction but only for frequencies lower than 0.1 Hz, whereas the buoy reproduces this component for frequencies higher than 0.1 Hz.

In this case for the frequency spectrum (Fig. 11) the WWIII model more adequately reproduces the significant wave height than SWAN model, but shows an underestimation (overestimation) of peak period (peak frequency) and a broader spectrum with less power concentrated in the vicinity of the peak period. The WWIII model exhibits a small peak of energy in the directional

spectrum at a low frequency (0.07 Hz approximately) but with a low spectral energy content (approximately 10% of the maximum energy), not reproduced by the buoy. The SWAN model in contrast has a narrower spectrum with higher levels of energy and a peak period less than that obtained by the buoy.

## 5. Summary and conclusions

Based on the results obtained for accurate blended wind as forcing for the most popular wind wave models (WWIII and SWAN) and directional and wave parameter data sets from NOAA buoy comparisons, the summary and conclusions are given in separate chapters:

**Blended winds:** This study clearly demonstrates that using realistic blended wind forcing and a high resolution WWIII model, successful simulations of the main wave parameters and directional spectrum in hurricane conditions may be generated. This confirms the benefits of employing simple methodologies that combine the advantages inherent in both reanalysis data sets and hurricane wind models, thereby permitting long term modeling.

**Wave parameters:** Comparisons between the WWIII and SWAN models showed that in the majority of the cases studied, and for most of the wave parameters (Hs, Tp, fp, Dirp), WWIII was in better agreement with the buoy data, confirming the results obtained by other authors.

**Spatial wave structure and quadrant location:** The WWIII model performs best for buoys located in the upper right front side of the storm track, which generally has higher winds and greater significant wave height values. This indicates that the WWIII model gives a better spatial representation of wave parameters in the higher energy areas of the hurricane.

Even for distant buoys, both models adequately reproduce the main characteristics related to distance from the hurricane center and the quadrant location, as has been presented by several authors. These characteristics are: (1) Higher and longer waves located in the right forward quadrant, with a narrow and unimodal spectrum propagating in the direction of the hurricane translation. (2) Smaller and shorter waves with more than one system (swell and sea) located in the left forward quadrant of the hurricane translation. (3) For incipient locations in the right upward quadrant, the directional spectrum presents a similar shape to that obtained in the right forward quadrant.

**Directional and frequency spectrum:** When comparing the values obtained by the WWIII and SWAN models, the results show how the SWAN model tends to overestimate the high frequency energy (also Reported by Ris et al., 1999; Rogers et al., (2003) and Bolaños-Sanchez et al., 2007, among others). On the contrary, using the parameterization of Tolman and Chalikov (1996) the WWIII model more adequately reproduces the spectrum for high frequencies (parametric tail) when compared with the values measured by the buoys.

The directional wave spectrum obtained by both models is quite similar, but the SWAN model tends to overestimate the significant wave height and the peak period. These results are in strong agreement with those obtained by other authors such as Ortiz and Mercado (2008), who attribute the difference in the models to the way wind energy is transferred to wave energy (Sin) and its dissipation due to whitecapping (Sds). For the general shape of the spectrum (directional spreading), numerical models showed similar results when compared with the buoy data for the analyzed cases, except for some high frequency components. Statistical analysis displayed less difference between the WWIII and SWAN models for the peak direction. These results are in agreement with those obtained by the three analyzed cases.

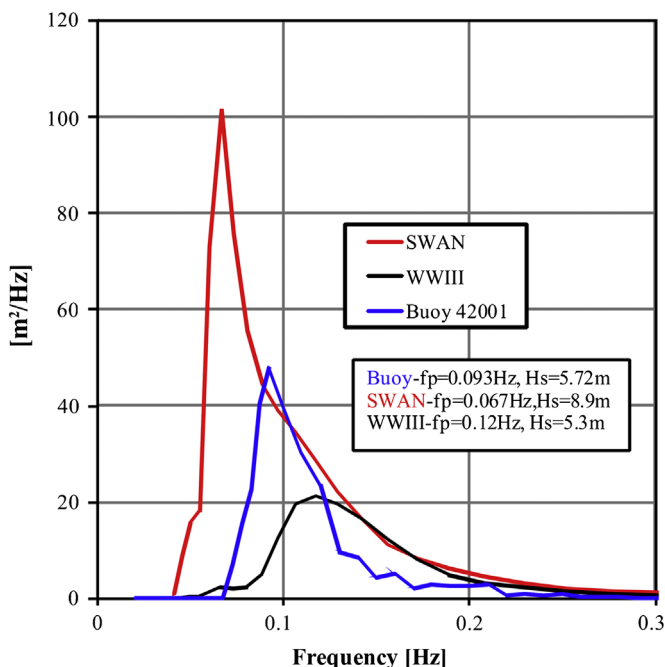


Fig. 11. Measured and predicted frequency spectrum for buoy 42001-Case 3. Buoy located at the rear left quadrant. During 20050829 00:00 UTC.

As mentioned by other researches, such results are very important considering the importance of the shape of the directional and frequency spectrum. They show that the tail of the spectrum has an important role in the wave spectral evolution and regarding the sensitivity to the directional distribution of the spectrum for non-linear interactions computed by a wave model (Rogers and Wang, 2006, Bolaños-Sánchez et al., 2007, among others).

**NOAA buoy directional spectrum:** For more energetic waves located in the right forward quadrant, although the method of Longuet-Higgins et al. (1963) is characterized by strongly increased directional spreading (as discussed above), it gives results consistent with the numerical models (SWAN and WWIII). However, for weak sea states the method has higher directional spread compared with the results obtained by the WWIII and SWAN models.

**Parameterizations:** The results obtained confirm those of Ortiz and Mercado (2008), for which the wind input parameterization in WWIII (Tolman and Chalikov, 1996) shows a better response to relatively fast changes in wind speed than the parameterization of Komen et al. (1984) used in SWAN.

Comparisons were made between the TC parameterization with and without limited drag (TCFLX3 and TCFLX2 respectively). A much better performance for significant wave height can be seen for the TCFLX2 parameterization. These results may be caused by the effect of using a limited drag coefficient for the TCFLX3 parameterization. As a consequence, underestimation is shown in the area of maximum winds generated by the reduction in the drag coefficient and thus in the Wind Input term (Sin). However, based on the high sensitivity of these results to wind accuracy for the entire structure of the hurricane, they should be used carefully. A comprehensive calibration process is recommended.

Comparing the results of the TCFLX2 parameterization with ACC350, it can be seen that both show very similar values of maximum significant wave height. However, the ACC350 parameterization tends to give greater values of significant wave height than TCFLX2 and TCFLX3 for most of the simulation time and most of the buoys. These results may be associated with the spatial structure obtained by ACC350, which tends to show a smaller spatial decrease in significant wave height outside the area of maximum winds. This is possibly induced by the drag limited behavior, which thereby generates an apparent overestimation around the eye of the hurricane compared to data observed by the in-situ buoys.

## Acknowledgments

The authors would like to thank NOAA that made the main data employed in this research freely available. They would also like to thank Dr. Pedro Osuna for his helpful contributions and Santiago Ortega, a Masters student of the Universidad Nacional (Medellin, Colombia), for his work on developing the SWAN data. Furthermore, they wish to thank Dr. Omar Lizano from the Universidad de Costa Rica for supplying the first version of the hurricane wind model HURWIN. Other acknowledgments go to COLCIENCIAS and the Universidad de Medellin for their economic support for Ph.D. development and to the project Research, analysis and assessment of erosion on the continental and Insular coast of the Colombian Caribbean, Special Agreement of Cooperation between the Instituto de Investigaciones Marinas y Costeras (INVEMAR) and COLCIENCIAS. This paper was written at the Universidad Nacional, Medellin, Colombia in support of Ruben Dario Montoya Ph.D. Support to F.J. Ocampo-Torres was provided by the CONACYT project RugDiSMarCTRLo-a (CONACYT-SEP grant 155793) and REDESCLIM.

## References

- Ardhuin, F., Magne, R., 2007. Current effects on scattering of surface gravity waves by bottom topography. *J. Fluid Mech* 576, 235–264.
- Ardhuin, F., Chapron, B., Collard, F., 2008. Ocean swell evolution from distant storms. *Nat. Geoscience*.
- Barber, N.F., Ursell, F., 1948. The generation and propagation of ocean waves and swell. *Philos. Trans. Roy. Soc. London* 240A, 527–560.
- Bidlot, J.R., Abdalla, S., Janssen, P.A.E.M., 2005. A Revised Formulation for Ocean Wave Dissipation in CY25R1. Tech. Rep. Memorandum R60.9/JB/0516, Research Department, ECMWF, Reading, UK.
- Bolaños-Sánchez, R., Sánchez-Arcilla, A., Cateura, J., 2007. Evaluation of two atmospheric models for wind-wave modelling in the NW Mediterranean. *J. Mar. Syst.* 65, 336–353.
- Booij, N., Holthuijsen, L.H., Ris, R.C., 1996. The “SWAN” wave model for shallow water. *Coastal Eng* 1, 668–672.
- Booij, N., Ris, R.C., Holthuijsen, L.H., 1999. A third-generation wave model for coastal regions. Part I. Model description and validation. *J. Geophys. Res.* 104 (C4), 7649–7666.
- Booij, N., 2004. SWAN Cycle III version 40.41 user manual. Available from: (<http://fluidmechanics.tudelft.nl/swan/index.htm>).
- Cardone, V.J., Cox, A.T., Greenwood, J.A., Thompson, E.F., 1994. Upgrade of Tropical Cyclone Surface Wind Field Model Misc. Paper CERC-94-14, US Army Corps of Engineers.
- Cavaleri, L., Sclavo, M., 2006. The calibration of wind and wave model data in the Mediterranean sea. *Coast. Eng.* 53, 613–627.
- Chao, Y.Y., Tolman, H.L., 2001. Specification of hurricane wind fields for ocean wave prediction. In: Edge, B.L., Hemsley, J.M. (Eds.), *Ocean Wave Meas. Anal. ASCE*, pp. 671–679.
- Chung-chu teng, Bouchard, R., Riley, R., Mettlich, T., Dinoso, R., Chaffin, J., 2009. NDBC's Digital Directional Wave Module. OCEANS, 2009, MTS/IEEE Biloxi-Maryne Technology for Our Future: Global and local changes.
- Collins, J.J., Viehnaman, J., 1971. A Simplified Empirical Model for Hurricane Wind Fields. Paper no. otc 1346. Offshore Technology Conference.
- Earle, M.D., 1996. Nondirectional and Directional Wave Data Analysis Procedures. NDBC technical Document, 96-01. National Data Buoy Center, Stennis Space Center, MS.
- Earle, M.D., Steele, K.E., Wang, D.W.C., 1999. Use of Advanced Directional Wave Spectra Analysis Methods. *Ocean Eng.* 26, 1421–1434.
- ECMWF, 2009. IFS Documentation Cy33r1, European Centre for Medium-Range Weather Forecasts ECMWF, ([www.ecmwf.int/research/ifsdocs/CY33r1/DYNAMICS/](http://www.ecmwf.int/research/ifsdocs/CY33r1/DYNAMICS/)).
- Guillaume, D., Xavier Bertin, X., Taborda, R., 2010. Wave climate variability in the North-East Atlantic ocean over the last six decades. *Ocean Modell.* 31, 120–131.
- Gunther, H., Hasselmann, S., Janssen, P.A.E.M., 1992. The WAM model Cycle 4 (revised version). *Deutsch. Klim. Rechenzentrum, Techn. Report no. 4*, Hamburg, Germany.
- Hasselmann, K., Barnett, T.P., Bouws, E., Carlson, H., Cartwright, D.E., Enke, K., Ewing, J.A., Gienapp, H., Hasselmann, D.E., Kruseman, P., Meerburg, A., Mueller, P., Olbers, D.J., Richter, K., Sell, W., Walden, H., 1973. Measurements of wind-wave growth and swell decay during the Joint North SeaWave Project (JONSWAP). *Ergaenzungsheft zur Deutschen Hydrographischen Zeitschrift, Reihe A* 8 (12), 95.
- Hasselmann, S., Hasselmann, K., Allender, J.H., Barnett, T.P., 1985. Computations and parameterizations of the nonlinear energy transfer in a gravity-wave spectrum. Part II: Parameterizations of the nonlinear energy transfer for application in wave models. *J. Phys. Oceanogr.* 15, 1378–1391.
- Holland, G.J., 1980. An analytical model of the wind and pressure profiles in hurricanes. *Mon. Wea. Rev.* 108, 1212–1218.
- Holthuijsen, L.H., Booij, H.N., 2003. Phase-decoupled refraction-diffraction for spectral wave models. *Coast. Eng.* 49, 291–305.
- Isobe, M., Kondo, K., Horikawa, K., 1984. Extension of MLM for estimating directional wave spectrum. In: *Proceedings of the Symposium on Description and Modeling of Directional Seas*, Lyngby, Denmark, Danish Hydraulic Institute, A-6-1-A-6-15.
- Janssen, P.A.E.M., 1989. Wind-induced stress and the drag of air-flow over sea waves. *J. Phys. Oceanogr.* 19, 745–754.
- Janssen, P.A.E.M., 1991a. Quasi-linear theory of wind wave generation applied to wave forecasting. *J. Phys. Oceanogr.* 21, 1631–1642.
- Janssen, P.A.E.M., 1991b. Consequences of the effect of surface gravity waves on the mean air flow. In: *International Union of Theoretical and Applied Mechanics (IUTAM)*, Sydney, Australia, 193–198.
- Jelenski, C.P., 1974. Special Program to List Amplitudes of Surges from Hurricanes (SPLASH); Part II: General tracks and variant storm conditions. NOAA, Tech. Memo., NWS TDL-52, Silver Spring.
- Khama, K., Hauser, D., Krogstad, H.E., Lenher, S., Monbaliu, J., Wyatt, 2003. Measuring and Analysing the Directional Wave Spectrum of Ocean Waves. COST 714 Working Group 3.
- Komen, G.J., Hasselmann, S., Hasselmann, K., 1984. On the existence of a fully developed wind-sea spectrum. *J. Phys. Oceanogr.* 14, 1271–1285.
- Komen, G.J.L., Donelan, M., Hasselmann, K., Hasselmann, S., Janssen, P.A.E.M., 1994. *Dynamics and Modelling of Ocean Waves*. Cambridge University Press, United Kingdom 532.
- Kreisel, G., 1949. Surface waves. *Quart. Journ. Appl. Math.* 21–44.

- Kudryavtsev, V.N., Makin, V.K., 2011. Impact of ocean spray on the dynamics of the marine atmospheric boundary layer. *Bound.-Layer Meteorol.* 140–3, 383–410.
- Ladd, C., Bond, N.A., 2002. Evaluation of the NCEP/NCAR reanalysis in the NE Pacific and the Bearing Sea. *J. Geophys. Res.* 107, C103158, <http://dx.doi.org/10.1029/2001JC001157>.
- Lizano, O.G., 1990. Wind model adjusted to a wave generation model for forecasting hurricanes. *Geophysics* 33, 75–103.
- Liu, H., Xie, L., Pietrafesa, L.J., Bao, S., 2007. Sensitivity of wind waves to hurricane wind characteristics. *Ocean Modell.* 18, 37–52.
- Longuet-Higgins, M.S., Cartwright, D.E., Smith, N.D., 1963. Observations of the directional spectrum of sea waves using the motions of a floating buoy. *Ocean Wave Spectra*. Prentice-Hall, Englewood Cliffs, NJ, pp. 111–136.
- Massel, S.R., 1996. Ocean surface waves: their physics and prediction. *Adv. Ocean Eng. World Scientific* 11, 494.
- Makin, V.K., 2005. A note on the drag of the sea surface at hurricane winds. *Boun.-Layer Meteorol.* 115, 169–176.
- Mesinger, F., DiMego, G., Kalnay, E., Mitchell, K., Shafran, P., Ebisuzaki, W., Jovic, D., Woollen, J., Rogers, E., Berbery E.H., Ek, M.B., Fan, Y., Grumbine, R., Higgins, W., Li, H., Lin, Y., Manikin, G., Parrish, D., Shi, W., 2006. North American Regional Reanalysis. *Bull. Amer. Meteor. Soc.*, 87, 343–360.
- Miles, J.W., 1957. On the generation of surface waves by shear flows. *J. Fluid Mech* 3 (2), 185–204.
- Moon, I.J., Ginis, I., Hara, T., Tolman, H.L., Wright, C.W., Walsh, E.J., 2003. Numerical simulation of sea surface directional wave spectra under hurricane wind forcing. *J. Phys. Oceanogr.* 33, 1680–1760.
- Mitsuyasu, H., 1968a. A note on the nonlinear energy transfer in the spectrum of windgenerated waves. *Rept. Res. Inst. Appl. Mech., Kyushu Univ* 16, 251264.
- Mitsuyasu, H., 1969. On the growth of the spectrum of windgenerated waves. II. *Rept. Res. Inst. Appl. Mech., Kyushu Univ* 17, 235–243.
- Moon, I.-J., Hara, T., Ginis, I., Belcher, S.E., Tolman, H., 2004a. Effect of surface waves on air–sea momentum exchange. Part I: Effect of mature and growing seas. *J. Atmos. Sci.* 61, 2321–2333.
- Moon, I.-J., Ginis, I., Hara, T., 2004b. Effect of surface waves on air–sea momentum exchange. Part II: Behavior of drag coefficient under tropical cyclones. *J. Atmos. Sci.* 61, 2334–2348.
- Moon, I.-J., Ginis, I., Hara, T., 2004c. Effect of surface waves on Charnock coefficient under tropical cyclones. *Geophys. Res. Lett.* 31, L20302.
- Montoya, R.D., Osorio, A., 2007. The wind wave models: characteristics, evolution and future applications in Colombia. *Adv. Water Resour.* 15, 47–74.
- Montoya, R.D., Osorio, A.F., 2009. Importance of Accurate Background Winds Combined with Hurricane Wind Models: Case Study of Hurricane Katrina. WISE meeting. Poster session. April 27 to April 30, 2009.
- Ochi, M.K., 1998. *Ocean Waves: The Stochastic Approach*. Cambridge University Press, United Kingdom, ISBN: 0-521-56378-X 319.
- Ortiz, J.C., Mercado, A., 2008. An intercomparison of SWAN and Wavewatch III models with Data from NDBC-NOAA buoys at oceanic scales. *Coast. Eng. J.* 50 (1), 47–73.
- Perlin, N., Samelson, R.M., Chelton, D.B., 2004. Scatterometer and model wind and wind stress in the Oregon–Northern California coastal zone. *Mon. Weather Rev.* 132, 2110–2129.
- Pickett, M.H., Tang, W., Rosenfeld, L.K., Wash, C.H., 2003. QuikSCAT satellite comparisons with nearshore buoy wind data off the US west coast. *J. Atmos. Oceanic Technol.* 20, 1869–1880.
- Phillips, O.M., 1957. On the generation of waves by turbulent wind. *J. Fluid Mech* 2 (5), 417–445.
- Phillips, O.M., 1958. The equilibrium range in the spectrum of wind-generated ocean waves. *J. Fluid Mech* 4, 426–434.
- Powell, M.D., Houston, S.H., Amat, L.R., Morisseau-LEROY, N., 1998. The HRD real time surface wind analysis system. *J. Wind Eng. Ind. Aerodyn.* 77–78, 53–64.
- Powell, M.K., Vickery, P.J., Reinhold, T.A., 2003. Reduced drag coefficient for high wind speeds in tropical cyclones. *Nature* 422, 279–283.
- Powell, M.D., Uhlhorn, W.E., Kepert, J., 2009. Estimating maximum surface winds from hurricane reconnaissance measurements. *Weather Forecast.* 24, 868–883.
- Powell, M.D., Murillo, S., Dodge, P., Uhlhorn, E., Gamache, J., Cardone, V., Cox, A., Otero, S., Carrasco, N., Annane, B., Fleur, R.St., 2010. Reconstruction of Hurricane Katrina's wind fields for storm surge and wave hindcasting. *Ocean Eng.* 37, 26–36.
- Rascle, N., Ardhuin, F. A global wave parameter database for geophysical applications. Part 2: Model validation with improved source term parameterization. *Ocean Modell.* 10.1016/j.ocemod.2012.12.001, in press. <http://dx.doi.org/10.1016/j.ocemod.2012.12.001>, in press.
- Reilly, W.C., Herbers, T.H.C., Seymour, R.J., Guza, T.T., 1996. A comparison of directional buoy and fixed platform measurements of pacific swell. *Atmos. Oceanic Technol.* 13 (1), 231–238.
- Ris, R.C., Holthuijsen, L.H., Booij, N., 1994. A spectral model for waves in the near shore zone. *Coast. Eng.* 1, 68–78.
- Ris, R.C., Holthuijsen, L.H., Booij, N., 1999. A thirdgeneration wave model for coastal regions. 2. Verification. *J. Geophys. Res.* 104, 7667–7681.
- Resio, D., Perrie, W., 1991. A numerical study of nonlinear energy fluxes due to wavewave interactions. Part I: Methodology and basic results. *J. Fluid Mech* 223, 609–629.
- Rogers, W.E., Hwang, P.A., Wang, D.W., 2003. Investigation of wave growth and decay in the swan model: three regional-scale applications. *J. Phys. Oceanogr.* 33, 366–389.
- Rogers, W.E., Wang, D.W.C., 2006. Directional validation of wave predictions. *J. Atmos. Oceanic Technol.* 24, 504–520.
- Ruti, P.M., Marullo, S., D'Ortenzio, F., Treantant, M., 2008. Comparison of analyzed and measurement wind speeds in the perspective of oceanic simulations over the Mediterranean basin: analysis, QuikSCAT and buoy data. *J. Mar. Syst.* 70, 33–48.
- Snyder, R.L., Cox, C.S., 1966. A field study of the wind generation of ocean waves. *J. Mar. Res.* 24, 141–178.
- Steele, K.E., Wang, D.W., 2004. Question of the pitch-roll buoy response to ocean waves as a simple harmonic oscillator? *Ocean Eng.* 31, 2121–2138.
- Steele, K.E., Wang, D.W., Earle, M.D., Michelena, E.D., Dagnall, R.J., 1999. Buoy pitch and roll computed using three angular rate sensors. *Coast. Eng.* 35, 123–139.
- Stockdon, H.F., Sallenger Jr, A.H., Holman, R.A., Howd, P.A., 2007. A simple model for the spatially-variable coastal response to hurricanes. *Mar. Geol.* 238, 1–20.
- Suzuki Isozaki, I., 1994. On the Development of A Global Ocean Wave Model JWA3G. *Proc. Pacific Ocean Remote Sensing Conference in Melbourne, Australia*, pp. 195–201.
- Swail, V.R., Cox, A.T., 2000. On the use of NCEP/NCAR reanalysis surface marine wind fields for long term North Atlantic wave hindcast. *J. Atmos. Oceanic Technol.* 17, 532–545.
- Tolman, H. L., 1989. The Numerical Model WAVEWATCH: A Third Generation Model for the Hindcasting of Wind Waves on Tides in Shelf Seas. *Communications on Hydraulic and Geotechnical Engineering, Delft Univ. of Techn., ISSN 0169-6548, Report no. 89-2*, 72 pp.
- Tolman, H.L., 1991a. A third-generation model for wind waves on slowly varying, unsteady and inhomogeneous depths and currents. *J. Phys. Oceanogr.* 21, 782–797.
- Tolman, H.L., 1992. Effects of numerics on the physics in a third-generation wind-wave model. *J. Phys. Oceanogr.* 22, 1095–1111.
- Tolman, H.L., Chalikov, D., 1996. Source terms in a third-generation wind-wave model. *Journal of Physical Oceanography* 26, 2497–2518.
- Tolman, 1999. User Manual and System Documentation of WAVEWATCH- III Version 1.18. Technical Note 166, Ocean Modeling Branch, NCEP, National Weather Service, NOAA, US Department of Commerce, 110 pp. Available from: <http://polar.wwb.noaa.gov/waves/wavewatch>.
- Tolman, H.L., 2002. User Manual and System Documentation of WAVEWATCH-III Version 2.22. Technical Note. Available from: <http://polar.ncep.noaa.gov/waves>.
- Tolman, H.L., 2002f. Validation of WAVEWATCH III Version 1.15 for a Global Domain. Technical Note 213, NOAA/NWS/NCEP/OMB, 33 pp.
- Tolman, H.L., 2009. User Manual and System Documentation of WAVEWATCH-III Version 3.14. Technical Note. Available from: <http://polar.ncep.noaa.gov/waves>.
- Tolman, H. L., 2002d. Testing of WAVEWATCH III Version 2.22 in NCEP's NWW3 Ocean Wave Model Suite. Technical Note 214, NOAA/NWS/NCEP/OMB, 99 pp.
- Tolman, H.L., Alves, J.H.G.M., 2005. Numerical modeling of wind waves generated by tropical cyclones using moving grids. *Ocean Modell.* 9, 305–323.
- Tracy, B., and Resio, D.T., 1982. Theory and Calculation of the Nonlinear Energy Transfer Between Sea Waves in Deep Water. WES Report 11, US Army Corps of Engineers.
- Ueno, K., Ishizaka, M., 1997. Efficient computational scheme of nonlinear energy transfer of wind waves. *Sokkojihou* 64, 75–80.
- Veerasamy, S., 2008. Comments on reexamination of tropical cyclone wind-pressure relationship. *Weather Forecast.* 23, 758–761.
- Walsh, E.J., Wright, C.W., Vandermark, D., Krabill, W.D., Garcia, A.W., Houston, S.H., Murillo, S.T., Powell, M.D., Black, P.G., Marks, F.D., 2001. Hurricane Directional Wave Spectrum Spatial Variation at Landfall. *J. Phys. Oceanogr.* 32 (6), 1667–1684.
- WAMDI Group (13 authors), 1988. The WAM model. A third generation ocean wave prediction model. *J. Phys. Oceanogr.* 18, 1775–1810.
- Wang, H.T., Freise, C.B., 1997. Error analysis of the directional wave spectra obtained by the NDBC 3-m pitch-roll disc buoy. *IEEE J. Oceanic Eng.* 22 (4), 639–648.
- Webb, D.J., 1978. Nonlinear transfers between sea waves. *DeepSea Res.* 25, 279–298.
- Willoughby, H.E., 2004. Parametric representation of the primary vortex. Part I: observations and evaluation of the Holland (1980) Model. *Monthly Weather Rev.*, 3033–3048.
- Wingert, K.M., Reilly, W.C.O., Herbers, T.H.C., Pwittmann, A., Janssen, R.E., Tolman, H.L., 2001. Validation of operational global wave prediction models with spectral buoy data. In: Edge, B.L., Hemsley, J.M. (Eds.), *Ocean Wave Meas. Anal.* ASCE, pp. 590–599.
- Wright, C.W., et al., 2001. Hurricane directional wave spectrum spatial variation in the open ocean. *J. Phys. Oceanogr.* 31, 2472–2488.
- Xu, F., Perrie, W., Toulany, B., Smith, P.C., 2007. Wind – generated waves in Hurricane Juan. *Ocean Modell.* 16, 188–205.
- Young, I.R., 2006. Directional spectra of hurricane wind waves. *J. Geophys. Res.* 111, C08020, <http://dx.doi.org/10.1029/2006JC003540>.
- Zhang, S., Zhang, J., 2005. A new approach to estimate directional spreading parameters of a Cosine-2s Model. *J. Atmos. Oceanic Technol.* Vol 23 (2), 287–301.
- Zhuo, L., Wang, A., Guo, P., 2008. Numerical simulation of sea surface directional wave spectra under typhoon wind forcing. *Export. J. Hydrodyn., Ser. B* 20 (6), 776–783.
- Zhang, H.M., Bates, J.J., Reynolds, R.W., 2006. Assessment of composite global sampling: sea surface wind speed. *Geophys. Res. Lett.* 33, L17714, <http://dx.doi.org/10.1029/2006GL027086>.